J. Fluid Mech. (2023), *vol*. 956, A33, doi:10.1017/jfm.2023.23

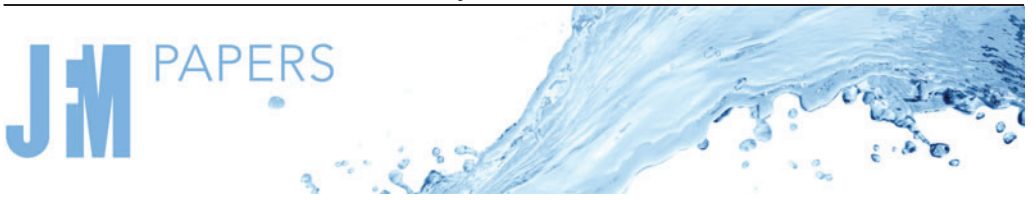

Disturbance growth in a laminar separation bubble subjected to free-stream turbulence

Tomek Jaroslawski[1],†, Maxime Forte[1], Olivier Vermeersch[1], Jean-Marc Moschetta[2] and Erwin R. Gowree[2]

[1]ONERA, DMPE, Universite de Toulouse, 31055 Toulouse, France

[2]ISAE-SUPAERO, Universite de Toulouse, 31055 Toulouse, France

(Received 15 April 2022; revised 18 November 2022; accepted 3 January 2023)

Experiments were conducted to study the transition and flow development in a laminar separation bubble (LSB) formed on an aerofoil. The effects of a wide range of free-stream turbulence intensity ($0.15\,\% < Tu < 6.26\,\%$) and streamwise integral length scale ($4.6\ \text{mm} < \Lambda_u < 17.2\ \text{mm}$) are considered. The co-existence of modal instability due to the LSB and non-modal instability caused by streaks generated by free-stream turbulence is observed. The flow field is measured using hot-wire anemometry, which showed that the presence of streaks in the boundary layer modifies the mean-flow topology of the bubble. These changes in the mean flow field result in the modification of the convective disturbance growth, where an increase in turbulence intensity is found to dampen the growth of the modal instability. For a relatively fixed level of Tu, the variation of Λ_u has modest effects. However, a slight advancement of the nonlinear growth of disturbances and eventual breakdown with the decrease in Λ_u is observed. The data show that the streamwise growth of the disturbance energy is exponential for the lowest levels of free-stream turbulence and gradually becomes algebraic as the level of free-stream turbulence increases. Once a critical turbulence intensity is reached, there is enough energy in the boundary layer to suppress the laminar separation bubble, resulting in the non-modal instability taking over the transition process. Linear stability analysis is conducted in the fore position of the LSB. It accurately models incipient disturbance growth, unstable frequencies and eigenfunctions for configurations subjected to turbulence intensity levels up to 3 %, showing that the mean-flow modification due to the non-modal instability dampens the modal instability.

Key words: boundary layer stability, boundary layer separation

† Email address for correspondence: tomek.jaroslawski@gmail.com

1. Introduction

At low Reynolds numbers ($Re_c < 5 \times 10^5$, based on the chord of the aerofoil and the free-stream velocity, $Re_c = U_\infty c/\nu$, where U_∞ is the freestream velocity, c the wing chord and ν the kinematic viscosity of the fluid), viscous effects are so significant that the presence of a strong enough adverse pressure gradient can cause a laminar boundary layer to separate from the wall. These flows occur in many engineering applications such as low-pressure turbines (Volino 1998) and micro-aerial vehicles (Jaroslawski *et al.* 2022). As a result of boundary layer separation, a laminar shear layer undergoes transition to turbulence, negatively impacting the noise emissions, lift, drag and unsteady loading of the aerodynamic surface (Carmichael 1981).

In a time-averaged sense, depending on the Reynolds number, angle of incidence and the amount of free-stream disturbance, the separated shear layer will remain separated or reattach to the wall. Gaster (1967) proposed a two-parameter criterion, considering a pressure-gradient parameter and a Reynolds number based on the momentum thickness at separation ($Re_{\delta_{2,sep}} = U_\infty \delta_{2,s}/\nu$, where $\delta_{2,s}$ is the momentum thickness at the separation point). For weakly adverse pressure gradients and high values of $Re_{\delta_{2,sep}}$, the separated shear layer will reattach as a turbulent boundary layer, forming a closed region of recirculating fluid, commonly referred to as a laminar separation bubble (LSB) or short bubble. With an increase in incidence or decrease in $Re_{\delta_{2,sep}}$, the separated shear layer may fail to reattach, and the short bubble may burst to form either a long bubble or an unattached free shear layer. In a low free-stream disturbance environment, the mechanisms of boundary layer transition in the separated shear layer are through the amplification of low-amplitude disturbances, where Diwan & Ramesh (2009) provided evidence that the origin of the inflectional instability in an LSB can be traced back to a region upstream of separation where the disturbances in the attached boundary layer are amplified through a viscous instability. Xu *et al.* (2017) showed similar behaviour in three-dimensional (3-D) confined separation bubbles, where the disturbance growth was strongly dependent on the initial disturbance, similarly to what was postulated by Diwan & Ramesh (2009), where the former's direct numerical simulations showed that the transition to turbulence would not occur without the presence of excitation, despite the base flow being highly inflected. The transition process in the separated shear layer involves the primary amplification of perturbations. It is credited to an inviscid Kelvin–Helmholtz (KH) instability in the fore portion of the bubble, which is modelled well with linear stability theory (LST) (Häggmark, Hildings & Henningson 2001; Rist & Maucher 2002; Marxen *et al.* 2003; Yarusevych & Kotsonis 2017; Kurelek, Kotsonis & Yarusevych 2018). Global instabilities can also exist in LSBs; for example, Rist & Maucher (2002) demonstrated through an analysis of 1-D velocity profiles that a reverse flow of 15 %–20 % of the free-stream velocity could result in a global oscillator due to absolute instability. Moreover, works by Rodríguez & Theofilis (2010), Rodríguez & Gennaro (2019) and Rodríguez, Gennaro & Souza (2021) also show global instability in LSBs, which are three-dimensional, at zero frequency and consist of a different mechanism than in Rist & Maucher (2002), resulting in lower reversal velocities ($\approx$7 %) triggering global instability. Rodríguez, Gennaro & Juniper (2013) compared these two types of global instabilities and confirmed the findings by Rist & Maucher (2002) and Rodríguez and co-workers. It should be noted that global instabilities have been investigated numerically in the aforementioned works in the absence of free-stream turbulence over flat plates with imposed pressure gradients.

In boundary-layer flows subjected to no pressure gradient, laminar to turbulent transition induced by free-stream turbulence (FST) follows a different transition mechanism than classical modal theory and is often referred to as 'bypass' transition, which was first used

by Morkovin (1985), referring to the bypassing of current knowledge of the transition mechanisms which was limited to modal theory at the time. However, since then, substantial efforts have been made to understand the transition process in wall-bounded flows subjected to FST. Klebanoff & Tidstrom (1972) brought the first physical understanding of transition induced by FST, where the presence of 3-D low-frequency fluctuations inside the laminar boundary layer led to fluctuations in the boundary-layer thickness, often thought of as thickening and thinning of the boundary layer. This distortion of the boundary layer is dominated by streamwise velocity fluctuations, resulting in longitudinal streaks. When the FST level is greater than 1 %, the unsteady streamwise streaks (known as Klebanoff modes) dominate the transition process, occurring at low frequencies (Arnal & Julien 1978) and having disturbance levels up to 10 % of the free-stream velocity (Westin *et al.* 1994). Streaks or Klebanoff modes form through the 'lift-up' mechanism, consisting of energy transfer between the wall-normal velocity fluctuations (v') and the streamwise velocity fluctuations (u'), resulting in the streamwise non-modal growth of disturbances inside the boundary layer (Volino 1998; Andersson, Berggren & Henningson 1999; Luchini 2000; Brandt, Schlatter & Henningson 2004; Nolan, Walsh & McEligot 2010). Consequently, the maximum value of the streamwise perturbation along the wall-normal direction occurs at a location corresponding to the middle of the boundary layer (Arnal & Julien 1978), in contrast to the near-wall location in modal transition, and was later theoretically explained by optimal perturbation theory (Andersson *et al.* 1999; Luchini 2000).

In transition experiments, FST is often generated by static uniform grids, where the growth of disturbances in the boundary layer is highly dependent on the turbulence generating grid (Westin *et al.* 1994; Kendall 1998). The integral length scale, which generally scales by the mesh size, M, can be considered the average energy-containing vortex's size and is an important parameter when investigating the mechanisms present in transition induced by FST. Hislop (1940) demonstrated that the integral length scale partially influenced the location of transition, reporting that the transition position would move downstream as the streamwise integral length scale (Λ_u) increased. In contrast, to the results first proposed by Hislop (1940), Jonáš, Mazur & Uruba (2000) and Brandt *et al.* (2004) demonstrated that the transition position moves upstream with an increase of Λ_u. More recently, based on a set of 42 grid configurations, Fransson & Shahinfar (2020) created a semi-empirical transition prediction model considering Λ_u and Tu at the leading edge of a flat plate, where Tu is the turbulence intensity. It was hypothesised that there exists an optimum ratio between the boundary-layer thickness at the transition location (δ_{tr}) and Λ_u, which promotes transition, stating that an increase in Λ_u would move the transition location upstream when $\Lambda_u < 3\delta_{tr}$, and *vice versa*. In general, they concluded that, for low Tu, the increase in Λ_u will advance the transition position and that for high levels of Tu, an increase in Λ_u would delay transition, and was recently confirmed with further experiments by Mamidala, Weingärtner & Fransson (2022). The complexity of free-stream turbulence-induced boundary-layer transition stems from the boundary layer thickness growing with the downstream distance. Since the FST decays and the integral length scales grow in the streamwise direction, the forcing on the boundary layer changes gradually in the streamwise direction.

The effects of FST and integral length scale on boundary layer transition in LSBs have not been addressed to the same extent as for attached boundary layers; notably, there is a lack of experimental results and the role of the integral length scales. Häggmark, Bakchinov & Alfredsson (2000) provided some of the first experimental results on the effects of grid-generated FST (with levels of 1.5 % at the leading edge) on an LSB

generated over a flat plate subjected to an adverse pressure gradient using hot-wire anemometry measurements. They found low-frequency streaky structures in the boundary layer upstream of the separation and in the separated shear layer from smoke visualisation and spectral analysis. No strong evidence for the existence of 2-D waves, which are typical for separation bubbles in an undisturbed environment, was found. More recently, Istvan & Yarusevych (2018) experimentally investigated the effects of FST (regular static grid, $Tu = 0.06\,\%$ to $1.99\,\%$) on an LSB formed over a NACA0018 aerofoil for chord-based Reynolds numbers of 80 000 and 150 000 using particle image velocimetry (PIV). They found that the bubble was highly sensitive to FST, and increasing the level leads to a thinner bubble and a decrease in its chordwise length due to a downstream shift of the separation point and an upstream shift of the reattachment point as in past experimental works (Burgmann & Schröder 2008; Olson *et al.* 2013). Istvan & Yarusevych (2018) concluded that the maximum spatial amplification of disturbances in the separated shear layer decreased with the increase in Tu, implying that the larger initial disturbances are solely responsible for the earlier transition and reattachment. Simoni *et al.* (2017) used PIV to characterise the effects of Reynolds number (40 000 to 90 000) and FST ($Tu = 0.65\,\%$ to $2.87\,\%$) on an LSB generated over a flat plate, finding similar mean-flow trends as Istvan & Yarusevych (2018). Moreover, Dellacasagrande *et al.* (2020) generated an empirical correlation for the transition onset Reynolds number based on pressure gradient and Tu. They hypothesised that the Reynolds number variation mainly drives the length scale associated with the KH vortices and in line with Burgmann & Schröder (2008), whereas increasing the intensity of the FST level shifts the onset of the shedding phenomenon upstream.

In LSBs subjected to sufficient levels of FST, the co-existence of modal and non-modal instabilities arises. Hosseinverdi & Fasel (2019) used direct numerical simulations (DNS) to investigate the role of isotropic FST (with intensities of $0.1\,\%$ to $3\,\%$) on the hydrodynamic instability mechanisms of an LSB. They proposed that the boundary layer transition process was made up of two mechanisms. The first consisted of low-frequency Klebanoff modes (streaks) induced by the FST, and the second was a KH instability enhanced by the FST. Depending on the level of FST, either one or both of these mechanisms would dominate the transition process. They found that the KH instability was triggered much earlier, and transition was enhanced, leading to a drastic reduction in the size of the separation bubble. The streamwise streaks (Klebanoff modes) prior to the separation location led to a faster breakdown of the KH vortices. They concluded that the energy carried by the Klebanoff modes increased with Tu, thus leading to a more significant reduction in the mean separated region. Other DNS studies by Wissink & Rodi (2006) (flat plate, counter form wall to for pressure gradient, $Tu = 1.5\,\%$) showed that the nature of the instability mechanisms changes from modal amplification due to the KH instability to amplification of streamwise streaks for elevated levels of FST. These streaks extend into the region of the laminar separated flow and initiate breakdown via the formation of turbulent spots. Experimentally, Istvan & Yarusevych (2018) found that at FST levels of $1.99\,\%$, streamwise streaks were inferred through the reduction of the spanwise wavelength of the shear layer roller, signifying the passage to non-modal instability. Additionally, Verdoya *et al.* (2021) conducted a novel proper orthogonal decomposition analysis of PIV data and found structures resembling streaks in the x–z plane. A recent large eddy simulation LES investigation by Li & Yang (2019) on a low-pressure turbine blade subjected to a leading edge turbulence intensity level of $Tu = 2.9\,\%$, suggested that the secondary instability breaking down into 3-D structures is 'bypassed' due to the high levels of FST.

The role of the integral length scale in the boundary-layer transition mechanisms in an LSB is seldom studied due to the experimental difficulty of controlling this parameter. However, numerical studies by Hosseinverdi & Fasel (2019) have shown that a FST level between $Tu = 0.1\,\%$–$2\,\%$ and varying the integral length scale in the range $0.9\delta_1 - 3\delta_1$ had minimal effects on the mean bubble size. Breuer (2018) conducted large eddy simulations on an aerofoil subjected to FST, finding that a decrease in the integral length scale advanced the transition position, which was attributed to the fact that the smaller scales could penetrate the shear layer more easily than larger scales, effectively increasing the receptivity.

The present work investigates the effects of forcing a LSB with an extensive range of Tu and Λ_u on the flow development, stability and transition of the bubble. Free-stream turbulence is generated, in a controlled manner, using a variety of regular and fractal grids set up so that the turbulence interacting with the bubble would be approximately isotropic and homogeneous. The aim is to investigate, experimentally, the co-existence of modal and non-modal growths of disturbances in the LSB, their interaction and their effects on the transition process. The flow field developing over a 2-D aerofoil is measured using hot-wire anemometry. Integral boundary-layer calculations are used to validate the baseline flow configuration. The FST is characterised in detail using a two-component hot-wire anemometer, before the leading edge and above the flow developing over the aerofoil, where the turbulence intensity, integral length scale and spectra are analysed. The detailed measurements of boundary-layer development allow the characterisation of the disturbance growth mechanisms inside the bubble and are accompanied by a linear stability analysis which models the convective growth of modal disturbances inside the bubble subjected to elevated levels of FST.

2. Experiments

2.1. *Wind tunnel set-up*

The experiments were conducted at atmospheric conditions in the ONERA Toulouse TRIN 2 subsonic wind tunnel. The wind tunnel has a contraction ratio of 16 and test section entrance dimensions of 0.3 m width $\times$ 0.4 m height and a total length of 2 m. The flow exits the test section through a diverging nozzle with an expansion ratio of 3. It is discharged through a noise reduction chamber, which aims to prevent pressure waves from the exit driving fan downstream from propagating upstream into the test section and possibly interfering with the receptivity of the aerofoil. As a result, the maximum FST level (measured near the leading edge of the aerofoil, cf. figure 1) in the test section with the aerofoil mounted was found to be below 0.15 % and is calculated by the integral of the power spectral density of the velocity signal over frequencies ranging from 3 Hz to 10 kHz. All experiments were conducted on an aluminium NACA 0015 aerofoil model with no boundary-layer trip on the pressure side. Studer *et al.* (2006), studied the same model, and demonstrated that the model mounted in the TRIN2 wind tunnel exhibited a quasi-bidimensional flow in the region of interest of the current experiments; without the use of any flow control strategies to reduce the thickness of the boundary layer developing over the wind tunnel walls. The model was mounted horizontally in the test section with the leading edge placed 1.44 m downstream of the test section inlet and had a chord length (c) and span of 0.3 and 0.4 m, respectively. For all test configurations, the Reynolds number was fixed at $Re_c = 125\,000$, corresponding to a free-stream velocity of $U_\infty \cong 6$ m s^{-1}. The angle of attack, AoA, was fixed to the same value throughout

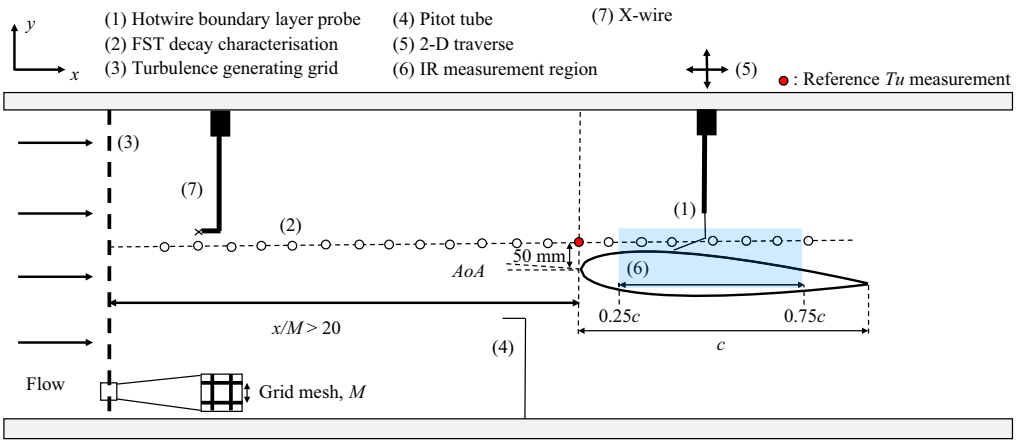

Figure 1. Experimental set-up. The reference turbulence intensity level and integral length scale are taken at the *Tu* reference measurement location (red marker), and are used to characterise each configuration for this study.

all experiments. An *AoA* of 2.3° was used as it allowed the traversing system to access all positions in the bubble while keeping the blockage ratio in the tunnel low. The experimental set-up is presented in figure 1.

2.2. *Boundary-layer and free-stream flow measurements*

Velocity measurements are acquired using a hot-wire probe mounted on a 2-D traverse. The probe's position in the streamwise, x, and wall-normal, y, directions is measured using Heidenhain LS388 linear encoders, with a stepping accuracy of 5 μm. Boundary layer measurements were made using constant temperature hot-wire anemometry (HWA) using a Dantec Dynamics Streamline Pro system with a 90C10 module and a 55P15 boundary-layer probe. To accurately evaluate the distance between the measurement probe and the wall, a camera equipped with a SIGMA 180 mm 1 : 3 : 5 APO-MACRO-DG-HSM-D lens and a 2× SIGMA EX teleconverter is used to set the zero for each boundary-layer profile measurement, where the closest measurements to the wall are taken at 200 μm, to avoid any near-wall correction, due to thermal effects between the wall and the hot-wire. Free-stream turbulence measurements were conducted using a 5 μm Dantec 55P51 probe, where a 6 mm diameter Dantec 55H24 support was used to support the X-wire probes. All test data were acquired using a National Instruments CompactDAQ-9178 with two NI-9239 (built-in resolution of 24 bit) modules for voltage measurements and a NI-9211 (built-in resolution of 16 bit) module for temperature measurements. Both single- and X-probes were calibrated *in situ* against a Pitot tube connected to an MKS 220DD pressure transducer. The boundary-layer probe (55P15) was calibrated using King's law (Bruun 1996) and the zero velocity voltage in the calibration was taken as the absolute minimum voltage measured over the sample duration with the wind tunnel off (Watmuff 1999). The X-wires (55P51) were calibrated for a velocity range of approximately 3–12 m s^{-1} and nine angles ranging between −28° and +28°. The velocities were obtained using the look-up table approach described by Burattini & Antonia (2005) and Lueptow, Breuer & Haritonidis (2004). Hot-wire drift was accounted for by conducting pre-and post- experiment calibrations. The frequency response of the system was estimated using the standard pulse-response test. It was approximately 45 kHz,

well above these experiments' spectral region of interest. The sampling frequency was set to $f_s = 25$ kHz where an anti-aliasing filter was automatically applied by the acquisition card. The sampling time was set so that second-order statistics would converge to at least ± 1 % at every location using the 95 % confidence interval (Benedict & Gould 1996). This resulted in mean profile measurements being conducted for 10 s for each point. The FST generated by the grids was characterised using the X-probe. Streamwise measurements were taken along the wind tunnel's centre line before the aerofoil's leading edge and 50 mm above the surface of the aerofoil. A stabilisation time of 10 s was used between traverse movements to ensure any vibrations from the movement had damped out. It should be noted that the purpose of this study was not a detailed investigation into the mechanisms of the decay of grid-generated turbulence. However, some care was taken in ensuring at least 40 000–60 000 integral lengths of the flow were measured (corresponding to a sampling time of approximately 120 s for each point) to obtain accurate converged statistics when characterising the FST generated by the grids. The uncertainty in hot-wire measurements was estimated to be less than 3 %, for $U/U_\infty > 0.2$ and the uncertainty in the hot-wire positioning is estimated to be less than 0.05 mm. The use of HWA in the study of LSBs is fraught with difficulty. In particular, the mean velocity measurement cannot detect the reverse flow region in the LSB. Furthermore, fluctuating velocity measurements are limited due to a non-negligible normal or spanwise component; however, it is not an issue for the amplification growth rate as the maximum value of fluctuations is outside the separated region. Nevertheless, as demonstrated by Boutilier & Yarusevych (2012), HWA can be used to study the transition mechanisms in an LSB. Spanwise measurements were not possible due to limitations in the experimental set-up, however, manually traversed spanwise measurements where conducted to verify the 2-D extent of the bubble. Finally, although not presented in the present paper, infrared thermography measurements (IRT) were conducted on the aerofoil's pressure side to verify the bubble's mean-flow topology. The IRT and manually traversed spanwise HWA measurements showed uniformity for $z/c = 0.08$ and 0.055, respectively.

2.3. *Characterisation of FST*

The FST is characterised by its intensity (Tu and Tv) and streamwise and vertical integral length scales (Λ_u and Λ_v, respectively). The integral length scale is the most energetic scale, corresponding to the average energy-containing vortex's average size. Other scales of turbulence consist of the Kolmogorov scale, the smallest viscous scale, and the Taylor length scale, the smallest energetic length scale in the turbulent flow, and are not believed to be important scales for the boundary-layer transition process (Fransson & Shahinfar 2020). Free-stream turbulence was generated using a variety of static turbulence generating grids. Different grid solidities (σ), mesh sizes (M), bar thicknesses (t) and relative distances between the grid and the leading edge can be used to vary the FST characteristics. In the present work, the values of σ were kept within limits recommended by Kurian & Fransson (2009), and M was varied to change the levels of turbulence intensity. Placing the grid closer to the leading edge leads to a lower integral length scale and higher turbulence intensity (Tu). The difficulty of keeping the FST level fixed while varying the scale was highlighted by Fransson & Shahinfar (2020). The streamwise position of the grids (for grids with $M = 6$ and 12 mm) is varied to change the value of the integral length scale while keeping the value of Tu relatively constant; a similar method has been used by Jonáš *et al.* (2000) and Fransson & Shahinfar (2020). All grids were placed at least $20M$ away from the leading edge of the aerofoil, ensuring the FST is relatively isotropic and

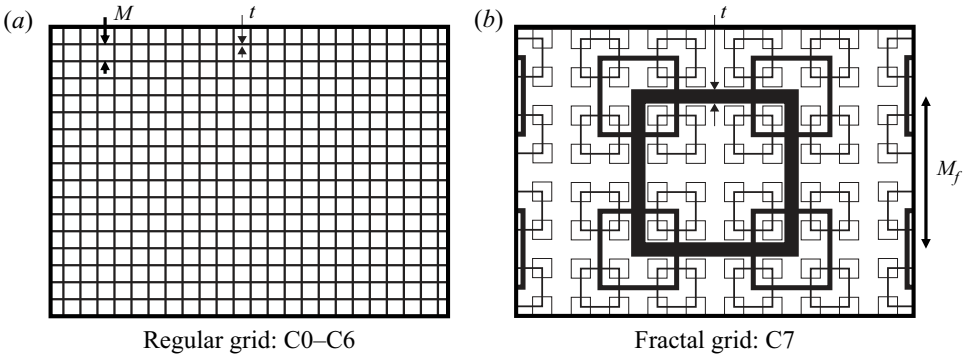

Figure 2. Schematics of grids used. (*a*) Regular grid (configs C0–C6) and (*b*) fractal grid (config. C7).

homogeneous. The values of Tu and Tv are defined in (2.1*a*,*b*)

$$Tu = \frac{u_{rms}}{U_\infty}, \quad Tv = \frac{v_{rms}}{U_\infty}. \tag{2.1a,b}$$

The values of Λ_u and Λ_v are calculated by integrating the autocorrelation of their fluctuating velocity signals and applying Taylor's hypothesis of frozen turbulence, which converts the time to spatial scales, and is presented in (2.2)

$$\Lambda_{u,v} = U_\infty \int_0^\infty f(\tau)\,\mathrm{d}\tau, \tag{2.2}$$

where $f(\tau)$ denotes the auto-correlation function of the signal and τ the time delay. The auto-correlation function was numerically integrated until the first zero crossing to obtain the integral length scale (Kurian & Fransson 2009). Experimental investigations of boundary layer transition induced by FST have used active grids to generate larger values of turbulence intensity and Λ_u, such as in Makita & Sassa (1991) and Fransson, Matsubara & Alfredsson (2005). The experimental implementation of these grids is costly, hence in the present work, a fractal grid was leveraged to generate high levels of turbulence intensity and length scales of turbulence under the condition that the grid is sufficiently far away from the leading edge such that the flow is more spatially homogeneous (Hurst & Vassilicos 2007). The present work does not consider investigations of the effects of non-equilibrium turbulence near the fractal grid. A summary of the grids tested in the current work can be found in table 1, with the schematics of the regular and fractal grids presented in figure 2.

The turbulence parameters relevant to the current investigation are summarised in table 2. The decay and evolution of the turbulence level, Tu, Tv and its integral length scales, Λ_u, Λ_v are presented in figures 3(*a*,*b*) and 3(*c*,*d*), respectively.In agreement with previous studies, from figure 3(*a*,*b*) exponential decay of Tu and Tv is present before the leading edge of the aerofoil, and the integral length scales increase in size moving further away from the grid. The development of the FST over the aerofoil shows that Tu is rather constant over the entire aerofoil, except for the highest Tu configurations where it still decreases near the leading edge. In zero-pressure-gradient boundary layers subjected to FST, Tu continues to decay in the streamwise direction (Jonáš *et al.* 2000; Brandt *et al.* 2004; Fransson *et al.* 2005), which is not the case in the present work as the favourable pressure gradient near the leading edge of the aerofoil could be responsible for this behaviour. From figure 3(*b*), it can be seen that, for configurations C1, C2 and C3,

Grid type	M (mm)	σ	t (mm)
Regular	3	36	0.6
Regular	6	31	1
Regular	12	44	3
Regular	50	33	9
Regular	70	36	14
Fractal	140	29	13

Table 1. Parameters of turbulence generating grids. The fractal grid is characterised by the size of the largest element, M_f.

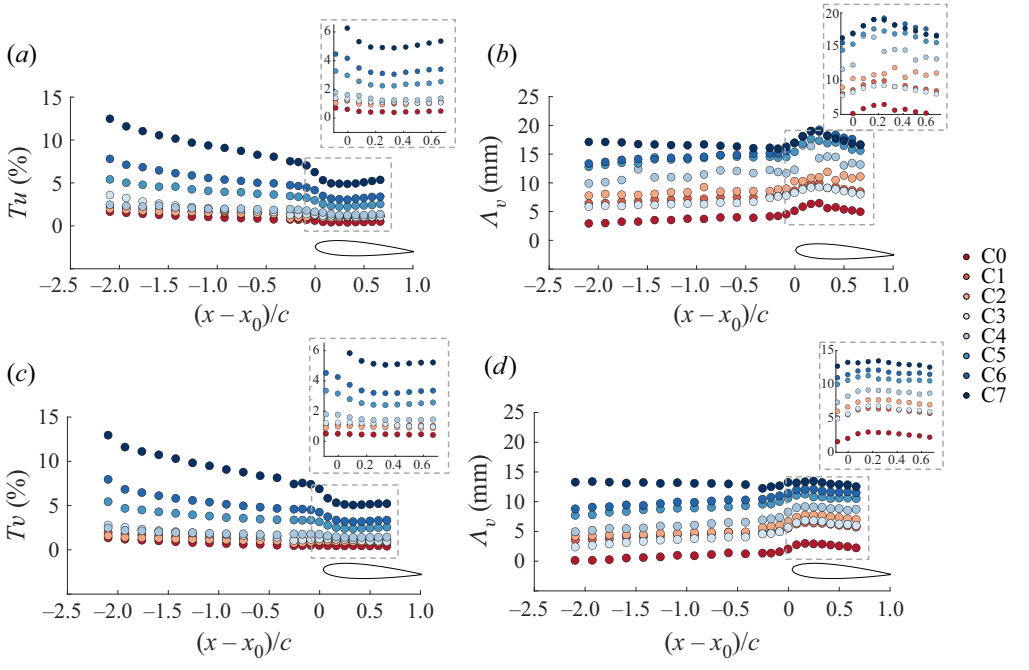

Figure 3. Streamwise evolution of Tu (a), Λ_u (b), Tv (c) and Λ_v (d) for FST configurations C0–C7.

Tu is relatively constant at the leading edge of the aerofoil with the integral length scales varying in the range 8.3–10.3 mm. The slight increase of the integral length scales after the leading edge could be due to the increased velocity near the leading edge of the aerofoil. This could suggest that the free-stream forcing on the boundary layer behaves differently in the present configuration than for a flat plate with zero pressure gradient; however, this is outside of the scope of this present work and has been recently investigated experimentally by Mamidala *et al.* (2022). Nevertheless, the current experimental characterisation of the FST behaviour before and around the aerofoil can serve as an input for future numerical studies. The power spectral density (PSD) of the FST is presented in figure 4, the inertial sub-range is largest for the configurations with the largest levels of Tu, coherent with the values of Λ_u and Λ_v.

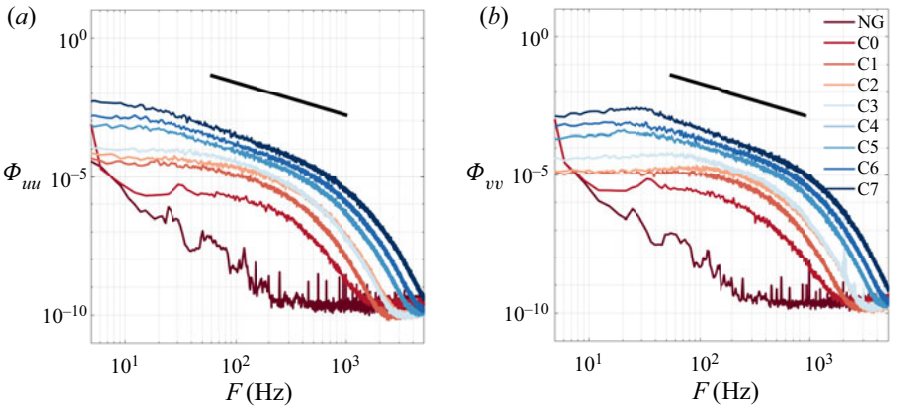

Figure 4. Power spectral density (Φ_{xx} [m^2 s^{-2} Hz^{-1}]) at the leading edge ($x/c = 0$) of the aerofoil. (*a*) Power spectral density for u' (Φ_{uu}) and (*b*) PSD for v' (Φ_{vv}).

Config.	v_{rms}/u_{rms}	Tu (%)	Λ_u (mm)	Λ_v (mm)	x/M
NG ●	0.92	0.15	210	181	—
C0 ●	0.82	0.64	4.6	3.1	480
C1 ●	0.91	1.21	8.7	5.5	143
C2 ●	0.81	1.23	10.3	6.7	240
C3 ●	0.92	1.31	8.3	5.6	138
C4 ●	1.07	1.63	12.3	8.3	120
C5 ●	1.07	2.97	15.4	10.6	29
C6 ●	1.02	4.16	16.8	11.4	21
C7 ●	1.10	6.26	17.2	13.3	—

Table 2. Free-stream turbulence test matrix. Turbulence isotropy, turbulence intensity (Tu), streamwise and vertical integral length scales (Λ_u and Λ_v, respectively) at the leading edge of the aerofoil ($x/c = 0$). Note that Λ_u and Λ_v are presented for the NG configuration for completeness, and are a result of the low disturbance flow, where the large length scales reflect a small perturbation to the mean flow.

3. Results

The results presented here pertain to experiments conducted on a NACA 0015 aerofoil at an angle of attack of 2.3° and Re_c of 125 000. For these conditions, the effects of FST and integral length scale on the transition process in an LSB are considered. The time-averaged flow is presented in § 3.1 followed by an unsteady analysis, instability and disturbance growth investigation in § 3.2.

3.1. *Time-averaged flow field*

3.1.1. *Baseline LSB*

Mean surface pressure measurements were conducted; however, the spacing of the pressure taps was too large to determine the streamwise positions of mean separation (x_S), transition (x_T) and reattachment (x_R). We note that the exact position of the separation is not critical for this study as the focus is on the instability characteristics, where the separation point is not a critical parameter when characterising the driving mechanism of the instability. However, as a good experimental practice, it was characterised

within the limits of the experimental set-up. Consequently, HWA measurements and numerical calculations were employed to characterise the baseline configuration. Measured boundary-layer profiles before x_S were independently validated using ONERA's in-house boundary-layer code 3C3D, which solves Prandtl's equations for 3-D boundary layers using a method of characteristics along local streamlines. The boundary-layer equations were set up using a body-fitted coordinate system, and the momentum equations are discretised along the local streamlines (Houdeville 1992). The streamwise pressure distribution serves as an input to the boundary-layer calculations. The interpolated measured pressure distribution and a numerical pressure distribution calculated with XFOIL (critical amplification factor, $N_{crit} = 6$) (Drela 1989) were used and found to yield close results. The boundary-layer solver stops marching at $x = 0.394c$ since no model for separated flows is implemented into the solver and corresponds to approximately x_S. Referring to figure 5, laminar boundary-layer profile development can be observed upstream of the separation point, with results from experiment and the boundary-layer solver showing a maximum difference of less than 7 % in the chordwise evolution of the integral parameters. No corrections were applied when calculating the experimental integral parameters. Mean velocity profiles downstream of the separation point exhibit reverse flow (although cannot be directly measured with HWA) near the wall and a profile inflection point at a vertical distance corresponding to the displacement thickness (δ_1), with the flow eventually reattaching as a turbulent boundary layer (cf. $x = 0.7c$, figure 5*b*). Moreover, relevant to linear stability (LST) calculations, the errors in mean velocity profiles, especially on those after separation and in the flow reversal region, have only a minor effect on the linear stability predictions of disturbance growth rates (Boutilier & Yarusevych 2012).

From HWA measurements, x_S is obtained by assuming that boundary layer separation occurs where $\partial U/\partial y = 0$, near the wall. In the present results, this location is determined to be $0.375c$, which agrees with that obtained from 3C3D, considering the spatial resolution of the HWA measurements would introduce an uncertainty of approximately $\pm 0.025c$. The experimental determination of x_S is often fraught with difficulty; hence, for this reason, separate IRT measurements were performed (not presented here) and it was found that separation occurs at approximately $0.36c$. Considering that the different values of x_s obtained from HWA, IRT and the boundary-layer solver have a standard deviation of $0.02c$, the error in the mean velocity sample from HWA and also considering a streamwise resolution uncertainty in the HWA measurements, the approximate uncertainty of x_s is $0.07c$.

The mean streamwise velocity contour in figure 6(*a*,*b*) shows the presence of a mean LSB that extends from $x_S/c = 0.375 \pm 0.07$ until $x_R/c = 0.700 \pm 0.025$. The bubble reaches its maximum height (x_H) at $x/c = 0.575 \pm 0.025$, where reasonable agreement has been found between maximum bubble height and mean transition position in previous work (Yarusevych & Kotsonis 2017; Kurelek *et al.* 2018), and will be used to define x_T for configurations with an LSB in the present work.

The streamwise unfiltered root-mean-square (r.m.s.) velocity field in figure 6(*b*) and profiles in the wall-normal direction in figure 5 show a gradual streamwise development of the fluctuations in the attached laminar boundary layer with a single peak near the wall emerging before the separation point, suggesting a viscous instability which has been sufficiently amplified to be detected by the measurement probe. Downstream, in the separated flow region, the spatial amplification of fluctuations increases rapidly in the laminar separation bubble, with a maximum at approximately $y/\delta_1 \approx 1$, which is in the vicinity of the inflection point. The u_{rms} profiles in the wall-normal direction exhibit

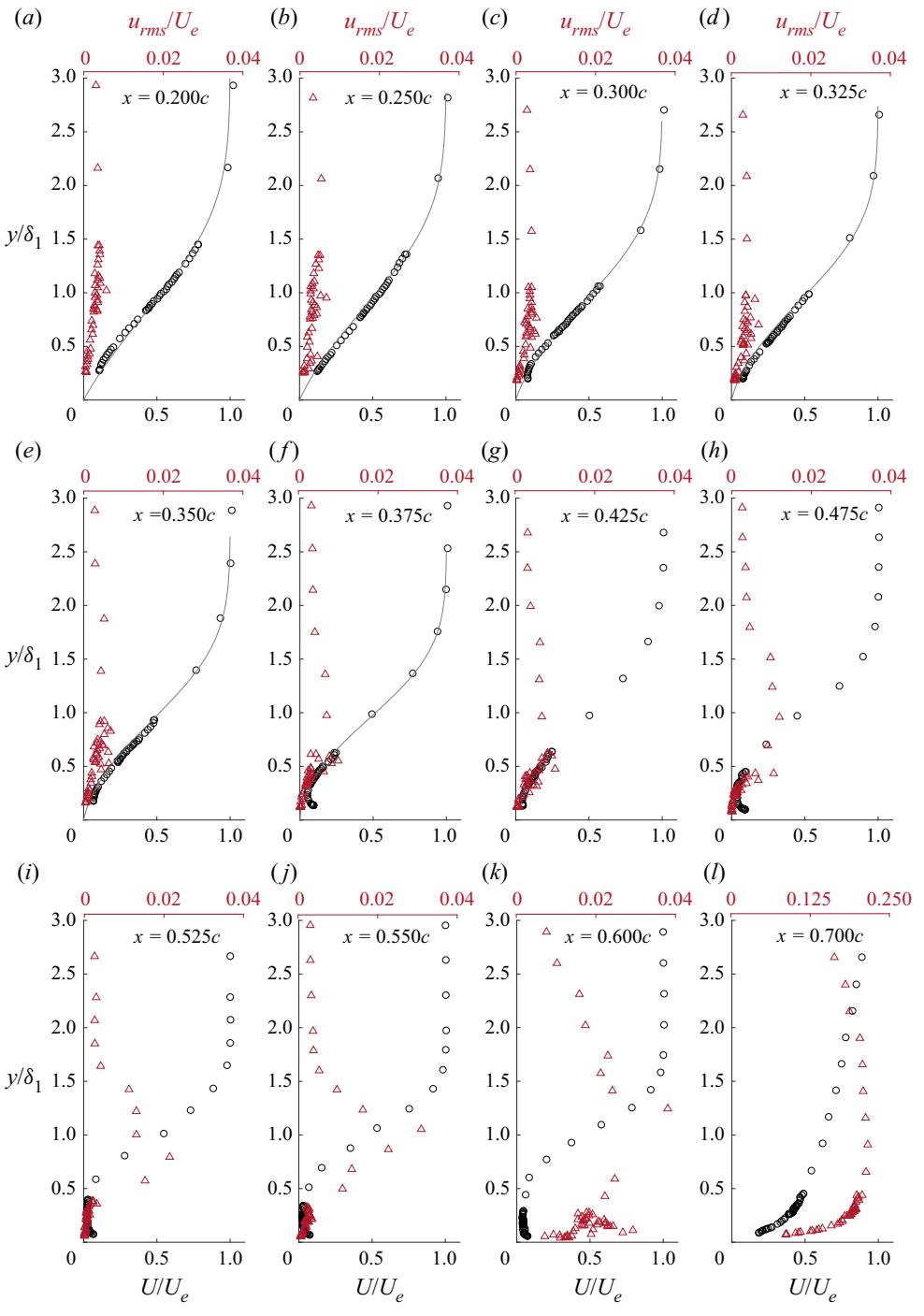

Figure 5. Chordwise evolution of the streamwise mean velocity (U) profiles and unfiltered u_{rms} profiles where markers represent experimental measurements, and the grey lines represent results obtained from 3C3D. After the separation point, x_s, 3C3D cannot calculate the boundary-layer profile and occurs at $x = 0.394c$. The wall-normal distance of each profile is scaled with the local value of δ_1.

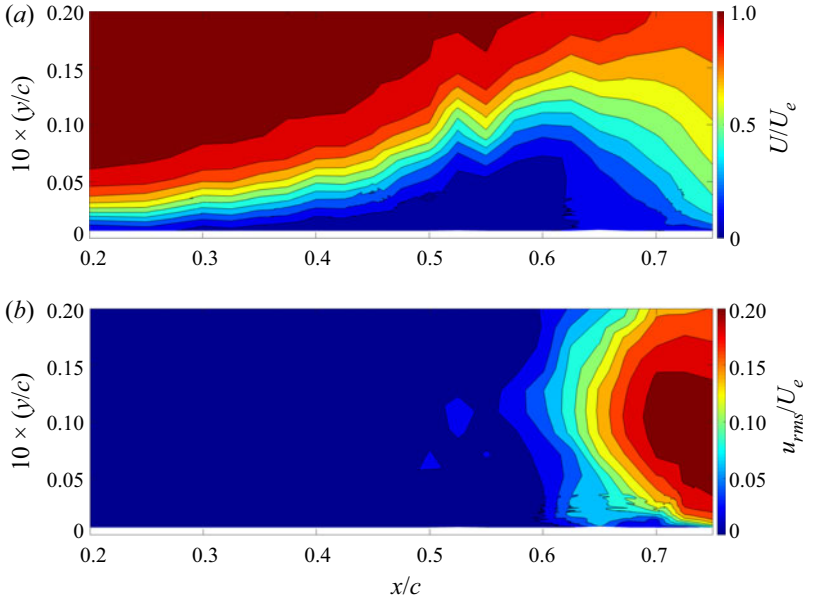

Figure 6. Contours (21 velocity profiles) of (*a*) the mean streamwise velocity (U) and (*b*) the r.m.s. of the fluctuating streamwise velocity (u_{rms}).

a multiple peak pattern inside the bubble, agreeing with Rist & Maucher (2002) just upstream of the reattachment position, showing the amplification of two near-wall peaks at $y/\delta_1 \approx 0.2$–0.5 and 1 (cf. figure 5). This indicates the growth of disturbances in the reserve flow region and separated shear layer with the latter following the displacement thickness (Kurelek *et al.* 2018). Qualitatively, the streamwise u_{rms} profiles are similar to a velocity fluctuation profile predicted by LST (Rist & Maucher 2002), indicating that the modal decomposition of these profiles could yield meaningful comparisons with LST. After turbulent reattachment, the u_{rms} profiles have a single peak near the wall (cf. figure 5 at $x/c = 0.7$) and diminish more gradually into the free stream than in the attached laminar boundary layer upstream, which is expected for a turbulent boundary layer (Diwan & Ramesh 2009; Boutilier 2011).

3.1.2. *Effect of FST intensity*

In the presence of FST forcing, the mean-flow topology of the LSB changes. In particular, a slight delay of boundary-layer separation is observed and the height of the LSB decreases significantly with the mean transition position advancing upstream, as can be observed in the contours of mean streamwise velocity and u_{rms} presented in figure 7. For the sake of brevity only three configurations are presented, C1 ($Tu = 1.21\,\%$), C5 ($Tu = 2.97\,\%$) and C7 ($Tu = 6.26\,\%$) where no LSB is observed. The measurements, in accordance with previous studies (Simoni *et al.* 2017; Istvan & Yarusevych 2018; Hosseinverdi & Fasel 2019), show that, with the increase of Tu, the streamwise extent of the separation bubble is reduced, as a result of an earlier onset of pressure recovery, caused by the shear layer transitioning in the aft position of the LSB. The length of the bubble decreases due to higher initial forcing or higher amplification rate. This has an impact on the reattachment point, leading to a shorter bubble. The displacement effect of the boundary layer will be reduced and will modify the pressure gradient and the re-adjustment results in the

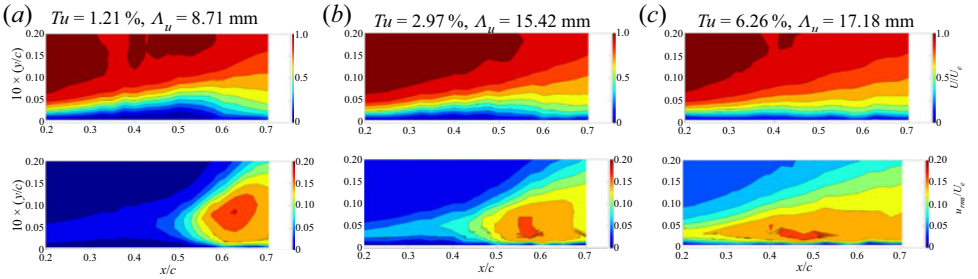

Figure 7. Contours of the mean streamwise velocity (U) and the r.m.s. of the fluctuating streamwise velocity (u_{rms}) for exemplary configurations subjected to elevated levels of FST (*a*) 1.21 % (*b*) 2.97 % and (*c*) 6.28 %.

small change in the location of the separation. This has been reported quite widely in the literature, where Marxen & Henningson (2011) have shown quantitative validation by varying the magnitude of initial perturbation. Finally, the height of the LSB is also reduced, and has been also observed in previous experimental and numerical studies (Simoni *et al.* 2017; Istvan & Yarusevych 2018; Hosseinverdi & Fasel 2019).

The delay in boundary-layer separation is thought to be due to the increased initial energy amplitude introduced into the boundary layer due to the FST, resulting in separation occurring further downstream, shortening the bubble due to the earlier transition. The resulting boundary-layer displacement effect modifies the upstream pressure field, leading to separation delay. The accurate quantification in the downstream shift of x_S with increased Tu is not possible here since it is smaller than the uncertainty in its determination. However, as mentioned in the previous section, the location of the separation position would have little impact on the boundary-layer transition mechanisms, hence it is not of great interest in the present study. The reattachment point is somewhat easier to determine, as its variation with Tu is larger than for the separation point since the inflectional nature of the profile is not clearly distinguishable. In the current configuration the reattachment point for the configurations where an LSB was observed are presented in table 3. Referring to the boundary-layer integral parameters presented in figure 8, the streamwise location of the peak in the displacement thickness (δ_1) is accompanied by an increase in momentum thickness (δ_2), and can be associated with the mean transition of the separated shear layer. Consequently, the shape factor ($H = \delta_1/\delta_2$) also reaches a maximum value at this position, corresponding to the maximum height of the LSB. Increasing the level of Tu results in a systematic decrease in δ_1, corresponding to the decrease in the wall-normal height of the LSB. Additionally, a higher Tu results in a less pronounced value of δ_1 and an upstream shift in the location of the maxima. This, combined with an earlier onset of momentum thickness growth, indicates earlier transition. When the levels of Tu pass a certain threshold, the existence of a LSB is in question as H does not exhibit any streamwise growth. In the current experimental configuration the level of Tu at which the bubble was suppressed is 4.26 % (C6). Configuration C5 ($Tu = 2.97$ %) could still have an LSB as an amplified frequency band is observed in the PSD and will be discussed in more detail in § 3.2. Furthermore, for all the configurations, H departs from a value expected for a laminar boundary layer ($H > 2.5$) and asymptotically levels off to that expected for a turbulent boundary layer ($H < 2$), signifying us that transition occurs within the HWA measurement domain. The current results exhibit the same systematic trends in mean bubble topology and integral parameters as in the DNS of Hosseinverdi & Fasel (2019) and PIV measurements of Istvan & Yarusevych (2018).

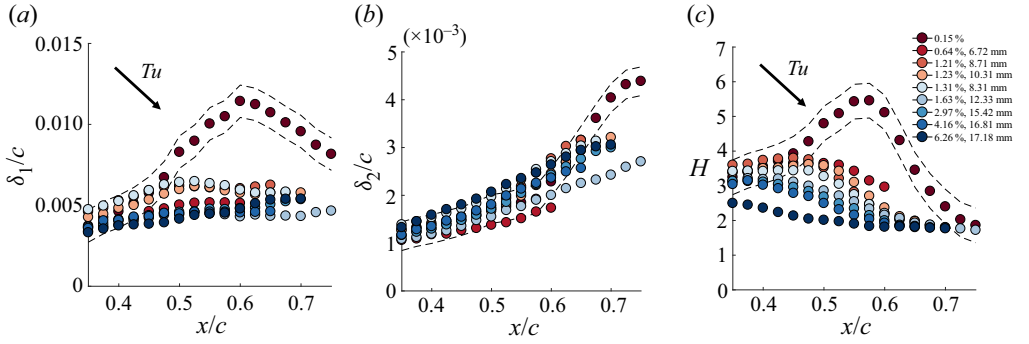

Figure 8. Effect of FST on integral shear layer parameters: (*a*) displacement thickness (δ_1), (*b*) momentum thickness (δ_2) and (*c*) shape factor (H). Turbulence intensity increases from dark red to dark blue, refer to table 2. Dashed lines denote uncertainty for the natural case.

Tu (%)	x_T/c	x_R/c
0.15	0.575	0.700
0.64	0.525	—
1.21	0.475	0.600
1.23	0.475	0.600
1.31	0.475	0.600
1.63	0.475	0.575
2.97	0.450	0.500

Table 3. Effect of FST on mean transition ($x_T/c \pm 0.025$) and reattachment ($x_R/c \pm 0.025$). The reattachment position was not measured in the configuration with $Tu = 0.64\,\%$.

Upon inspection of the u_{rms} profiles in the wall-normal direction from figure 9, increasing the Tu results in an upward shift in the maxima when compared with the baseline case. This behaviour suggests a shift in the transition mechanism, where a non-modal instability would exhibit the maximum u_{rms} values further away from the wall than a modal instability. Moreover, increasing the FST intensity yields magnitudes of $u_{rms}/U_e \approx 10\,\%$ which is common for streaks (Westin *et al.* 1994; Fransson *et al.* 2005), and is larger than what is observed for pure modal transition ($u_{rms}/U_e \approx 1\,\%$, Arnal & Julien 1978). The co-existence of modal and non-modal instabilities in attached boundary layers has been found to have similar effects on the maximum of the u_{rms} peak (Veerasamy, Atkin & Ponnusami 2021). Moreover, increasing Tu decreases the rate at which the fluctuations diminish into the free stream. In the configurations where Tu is large enough to suppress the bubble, the u_{rms} peak gradually shifts downwards, suggesting the flow is undergoing a change in transition mechanism and will be discussed later.

Using acoustic forcing, Kurelek *et al.* (2018) found that the initially increased amplitude in the boundary layer upstream of the flow resulted in the bubble being shorter and thinner, similar to what has been observed in Marxen & Henningson (2011) in DNS simulations. In the same manner, FST increases the initial forcing in the boundary layer, resulting in similar effects on the mean-flow topology as with different forcing techniques. The impact forcing has on the bubble is that it modifies the wall-normal height, which would have an effect on the modal instability mechanism in the separated boundary-layer profile. The eigenfunctions can recover features of both Tollmien–Schlichting and KH instabilities

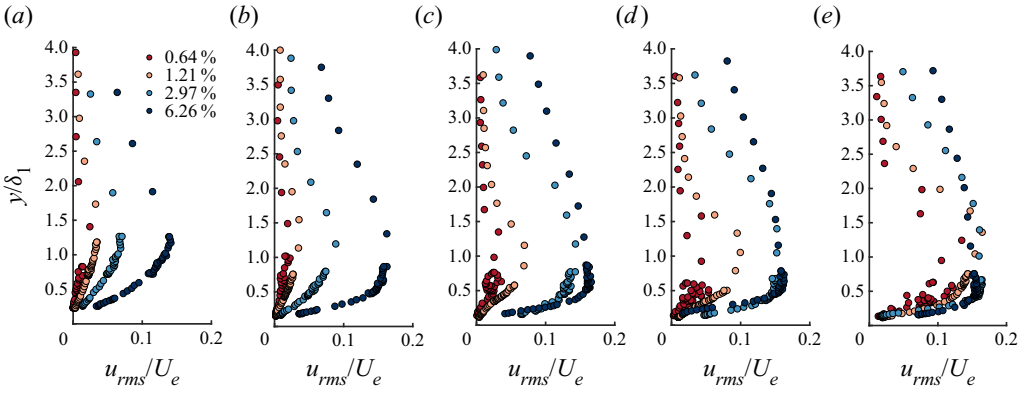

Figure 9. Chordwise development of the r.m.s. of the fluctuating streamwise velocity component (u_{rms}) for chordwise positions of (*a*) 0.250*c* (*b*) 0.350*c* (*c*) 0.425*c* (*d*) 0.500*c* and (*e*) 0.575*c* subjected to FST.

where the bubble's height can modify the two mechanisms' relative importance (Rist & Maucher 2002).

3.2. *Disturbance growth and instability*

3.2.1. *Spectral analysis*

The PSD of the streamwise velocity fluctuations was calculated for each configuration, with the chordwise evolution presented in figure 10. In the cases where an LSB was present, the PSD exhibits a characteristic frequency band amplified downstream (cf. figure 10*a–g*). When the LSB was subjected to FST, the chordwise development and distribution of the spectra were significantly modified. First, the unstable frequency band is broadened, which is a consequence of significant energy content within a larger range of frequencies in the FST, resulting in measurable velocity fluctuations over a larger frequency range earlier upstream. Second, increasing the FST level results in the unstable frequency band being slightly shifted to a higher frequency range than the natural case. For example, increasing the FST level from the baseline to a value of $Tu = 1.23\,\%$ results in the frequency band being shifted from 110–150 to 160–200 Hz (cf. figure 10*a*,*d*). Referring to figure 10(*a–g*), the unstable frequency band is propagated upstream of the separation point due to the separation bubble's streamwise oscillation. The highest-frequency wave packet is found to occur in the highest *Tu* case, which was 255–295 Hz, wherein the highest cases ($Tu > 4\,\%$, figure 10*h*,*i*) no clear frequency band is observed and is thought to be due to the LSB not being present anymore, implying a change in the instability mechanism. The frequency shift of the wave packet is attributed to the decreased size of the LSB and has been observed in Hosseinverdi & Fasel (2019). Current results suggest that, in the configurations that are subjected to a turbulence intensity of $Tu < 3\,\%$, the harmonic of the frequency band is still observed (cf. figure 10*b*,*f*,*e*), which could suggest that, in the presence of moderate levels of FST, the secondary instability of the primary modal instability could still be present. The secondary instability is a harmonic of the primary modal instability and takes effect in the aft portion of the bubble where vortex shedding occurs. In past studies, it has been reported to be an elliptic instability (Marxen, Lang & Rist 2013), amplifying disturbances with spanwise wavelengths of the order of the size of the shed vortices, resulting in spanwise distortion and waviness in the vortex filament and the presence of streaks could have an effect on this mechanism. The current results

indicate that if Tu is increased to a certain level, the harmonic of the wave packet is barely noticeable (cf. figure 10g), suggesting that there is a certain threshold of FST forcing which will 'bypass' the secondary instability, which will still exist in moderate cases and is in agreement with the numerical simulations of Li & Yang (2019). Finally, the impact of the integral length scale has a negligible effect on the unstable frequency range of the wave packet.

Pauley, Moin & Reynolds (1990) proposed a scaling of the most unstable frequency in an LSB, in the form of a Strouhal number defined as

$$St_{\delta_2,sep} = \frac{F\delta_{2,s}}{U_{e,s}}, \tag{3.1}$$

where F is the most amplified frequency observed in the experiment, $\delta_{2,s}$ and $U_{e,s}$ are the momentum thickness and boundary-layer edge velocity at separation, respectively. Inspired by the analysis of Rodríguez & Gennaro (2019) and Rodríguez *et al.* (2021), who compared the value of $St_{\delta_{2,sep}}$ for past experiments on LSBs, figure 11 compares the value of $St_{\delta_{2,sep}}$ as a function of Tu (for the cases where an LSB was observed). In the present work, $St_{\delta_{2,sep}} = 0.0062$ for the unforced bubble which is close to the value of $St_{\delta_{2,sep}} = 0.0069$ proposed by Pauley *et al.* (1990) for 2-D numerical simulations of an LSB. However, increasing Tu causes $St_{\delta_{2,sep}}$ to increase compared with the baseline case, approaching values closer to what was proposed by Rodríguez *et al.* (2021) of $St_{\delta_{2,sep}} =$ 0.01–0.012 for a bubble acting as a global oscillator. Data from Istvan & Yarusevych (2018) also suggest this effect and Pauley (1994) found that $St_{\delta_{2,sep}} = 0.0124$–$0.0136$ in 3-D unforced numerical simulations twice as large of what was observed for 2-D simulations. Therefore, the increased values of $St_{\delta_{2,sep}}$ suggests that the presence of FST (or increased levels of forcing) could favour the inherent 3-D nature of the transition process in the LSB. Furthermore, Rodríguez & Gennaro (2019) found that increasing the recirculating velocity in the bubble increased the values of $St_{\delta_{2,sep}}$ which could manifest here as well, since the LSBs subjected to FST are smaller in size for the same convective velocity, which would result in larger levels of re-circulation inside the bubble. Finally, discrepancies in the values of $St_{\delta_{2,sep}}$ can be associated with the set-up and configurations of experiments. For instance, flat plates (with imposed pressure gradients) vs aerofoils, the surface finish of the models, and the inherent bias of the different experimental techniques. Moreover, the different Reynolds numbers and pressure gradients would modify the mean bubble's height and length, which could also result in the differences in the value of $St_{\delta_{2,sep}}$. In particular, under certain conditions (Gaster 1967), the formation of a 'long' bubble can occur. However, it is outside of the scope of the current study, which focuses on a 'short' bubble.

The intermittent global motion of the separated shear layer in an LSB is often referred to as flapping and is known to occur at significantly lower frequencies than 2-D vortex roll-up and shedding (Zaman, McKinzie & Rumsey 1989; Michelis, Yarusevych & Kotsonis 2017), depending on the incoming perturbations, which can change the bubble's stability characteristics. Following the conventions from Michelis *et al.* (2017), the frequency normalised by the Strouhal number based on the displacement thickness

$$St_{\delta_1,sep} = \frac{F\delta_{1,s}}{U_{e,s}}. \tag{3.2}$$

We note that this Strouhal number should not be confused with the Strouhal number proposed by Pauley *et al.* (1990). Moreover, for assessing flapping experimentally, a

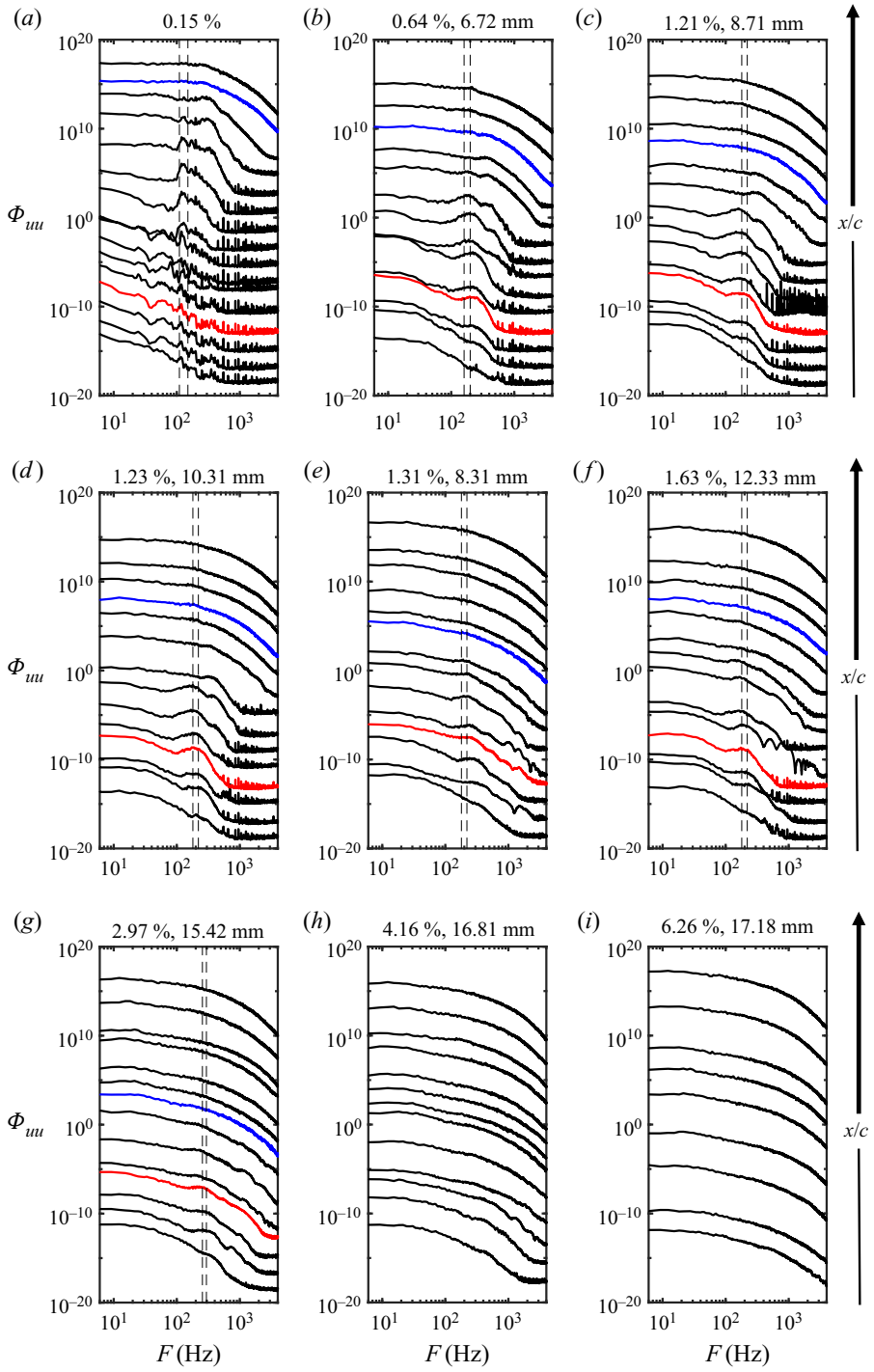

Figure 10. Chordwise evolution of the PSD of the streamwise velocity fluctuations at the maximum location of u_{max} inside the boundary layer for each configuration. The frequency bands correspond to the vertical dashed lines which indicate the most amplified frequency band used in the stability analysis in the following section. Red and blue curves denote x_S and x_R, respectively. NB: spectra are separated by an order of magnitude for clarity.

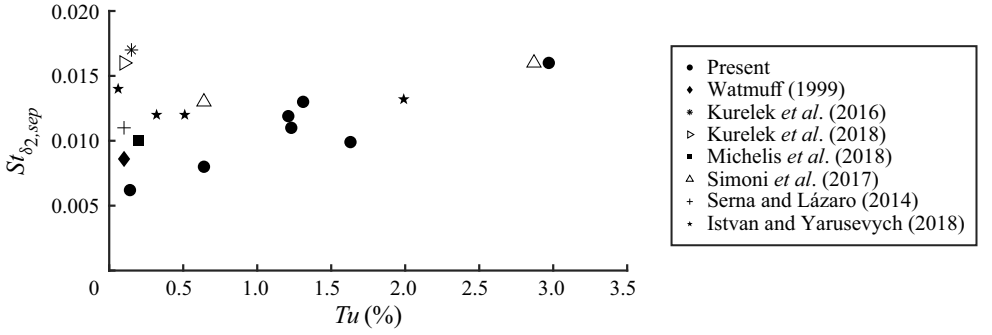

Figure 11. The dimensionless frequency, $St_{\delta_{2,sep}}$, plotted against the turbulence intensity, Tu, for the present results and experimental data from the literature.

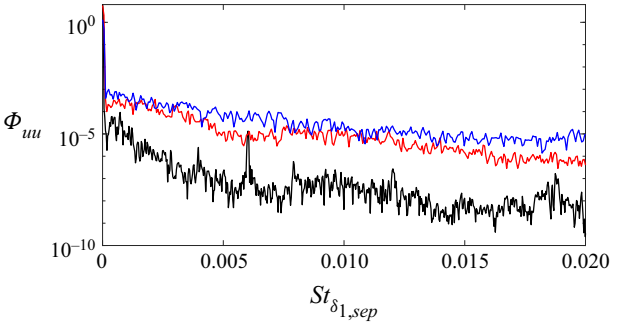

Figure 12. The PSD of the streamwise velocity fluctuations for the unforced LSB (black), the LSB subjected to $Tu = 0.64\,\%$ (red) and $Tu = 1.21\,\%$ (blue) at a height of $y = \delta_1$ at the separation point. The Strouhal number is scaled by δ_1, and should not be confused with the Strouhal number scaled with δ_2 in figure 11.

temporal signal is extracted at a streamwise location corresponding to the approximate position of the mean separation point, x_s, and at a wall-normal location of $y = \delta_1$. At this same position in the LSB, Michelis *et al.* (2017) demonstrated that the flapping of an unforced LSB manifested itself at low frequencies below $St_{\delta_{1,sep}} = 0.005$. The results shown in figure 12 suggest that flapping is also manifesting as we observe an increase in spectral content when $St_{\delta_{1,sep}} < 0.005$. When the Tu level is above the baseline, the increase of spectral content is less evident, suggesting that the level of free-stream disturbance could affect bubble flapping.

3.2.2. *Disturbance energy growth*

The effect of increasing the level of Tu on the chordwise evolution of the disturbance energy growth ($E = u_{rms}^2/U_e^2$) is presented in figure 13(a), where the trend of disturbance growth gradually changes from exponential, at lower levels of Tu, to algebraic for the more extreme Tu levels, where energy saturation is observed earlier. These different energy growth behaviours suggest that different instability mechanisms were present in the flow, and their contribution to the transition process depends on the level of the free-stream forcing. Figure 13(b) shows the energy growth of the filtered disturbances for the most amplified frequency band (corresponding to the modal instability in the LSB) obtained from the PSD (cf. figure 10). In the natural case, low levels of disturbance growth are present before the separation point, and further downstream, exponential amplification of

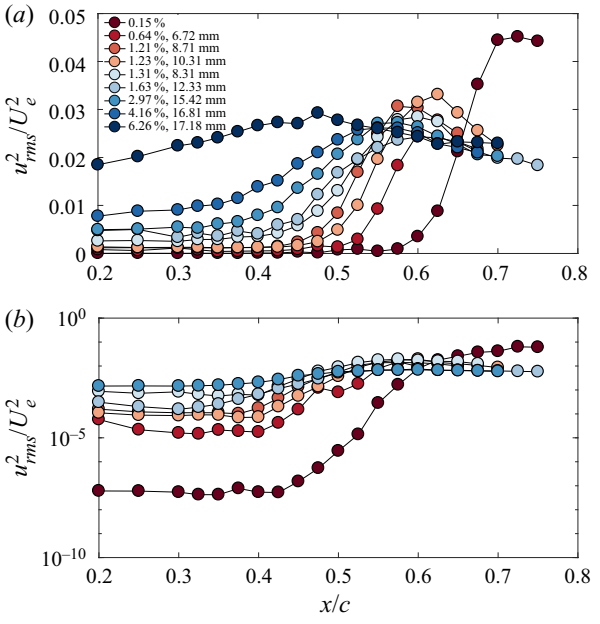

Figure 13. Energy growth of disturbances for (*a*) integrated over the entire energy spectrum and (*b*) integrated over the frequency range of the most amplified wave packet plotted on a semi-log scale to show modal growth. Configurations where no LSB was detected, i.e. where no amplified frequency band was observed in the PSD, are not included for the filtered disturbance growth (cf. figure 10*h*,*i*). Maximum values of u_{rms} in the boundary layer are presented.

the disturbances is observed. In the cases where the flow is subjected to additional FST, the initial energy amplitude is significantly higher than in the natural case. The initial energy in the boundary layer increases with *Tu*, with higher energy levels suggesting the presence of streaks, as commonly observed in experiments on transition induced by FST in boundary layers subjected to no adverse pressure gradient.

Referring to figure 13(*b*), the gradual reduction in the slope of the chordwise energy growth with increasing *Tu* would suggest that the non-modal instabilities become more dominant, which can be thought of as being in competition with the modal instabilities which grow exponentially. Once the turbulence forcing reaches a critical level, the exciting streaks in the boundary layer are too energetic to allow the flow to separate, resulting in the elimination of the modal via the non-modal instability (in the present work, approximately when $Tu > 4\,\%$, since no inflection point is observed in the mean flow and no amplified frequency band in the PSD). Damping of the modal disturbance growth is attributed to the mean-flow deformation due to the influence of FST. In other words, external FST forcing reduces the size of the separation bubble, such that the region of instability growth is brought closer to the wall, resulting in damping effects of the disturbances in the shear layer. Previous experiments on forced bubbles found a damping effect on the disturbance growth. For example, Kurelek *et al.* (2018) found that both tonal and broadband acoustic forcing resulted in the damping of modal disturbances along with Yarusevych & Kotsonis (2017) and Marxen & Henningson (2011) who used a variety of forcing techniques and observed similar behaviour. Furthermore, the DNS investigation by Hosseinverdi & Fasel (2019) found similar trends in the energy growth with increased levels of *Tu*, albeit they did not show the behaviour when the bubble was suppressed, which in the present results is

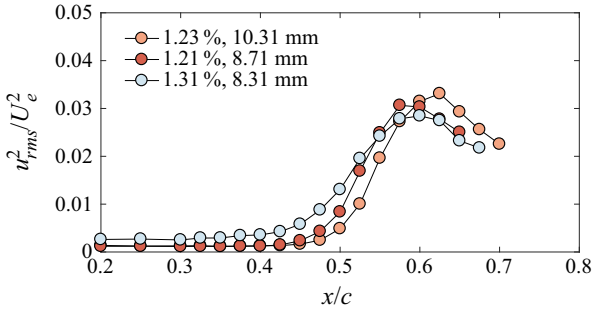

Figure 14. The chordwise evolution of the disturbance energy growth for configurations with a relatively fixed Tu and varying Λ_u. Maximum values of u_{rms} in the boundary layer are presented.

characterised by a high level of initial energy and evident algebraic growth of disturbances upstream of any possible separation location ($Tu = 6.26\,\%$, figure 13*a*).

The damping of the modal disturbances in the bubble could be due to the presence of streaks (Klebanoff modes) caused by the elevated levels of FST, which would introduce non-modal disturbances into the boundary layer. In the current set-up, streaks should appear for configurations where $Tu > 1\,\%$, which is a common threshold for zero-pressure-gradient boundary layers (Matsubara & Alfredsson 2001; Fransson *et al.* 2005). The behaviour of the disturbance growth suggests the co-existence of modal and non-modal instability in the LSB when subjected to a critical level of FST. The experimental findings here agree with previous numerical results in the literature (Balzer & Fasel 2016; Hosseinverdi & Fasel 2019; Li & Yang 2019).

The impact of the integral length scale for a relatively constant Tu level on the disturbance growth is presented in figure 14, suggesting that the effect of the integral length scale on the transition in an LSB is very modest. The difficulty in achieving constant levels of Tu with a varying Λ_u is an experimental challenge, as shown by Fransson & Shahinfar (2020). The present work investigates three cases with a minimal variation in Tu and a larger variation in Λ_u. It is observed that an increase in Λ_u at the leading edge of the aerofoil for an almost constant Tu appears to delay the growth and eventual saturation and breakdown of the disturbances and is in agreement Breuer (2018), who suggested that the smaller scales were closer to that of the shear layer resulting in the receptivity of the boundary layer increasing. The impact of Λ_u has been shown to have contradicting results in attached boundary-layer transition problems, where a variation of the integral length scale both advances (Jonáš *et al.* 2000; Brandt *et al.* 2004; Ovchinnikov, Choudhari & Piomelli 2008) and delays (Hislop 1940; Fransson & Shahinfar 2020) boundary-layer transition. This contradiction led Fransson & Shahinfar (2020) to hypothesise a twofold effect of the integral length scale on boundary-layer transition subjected to FST. They found that, for a constant Tu level, an optimal scale ratio exists between Λ_u at the leading edge and the boundary-layer thickness at the transition position, which has a value of approximately 15. Interestingly, in the attached portion of the boundary layer of the three configurations tested, the advancement of the nonlinear growth of disturbances and eventual breakdown occurs when approaching this optimal value.

However, it should be noted that the above studies were conducted on attached boundary layers. Hence, it is unclear whether meaningful comparisons can be made. For LSBs, Hosseinverdi & Fasel (2019) briefly suggested that the integral length scales ranging from $0.9\delta_1$ to $3\delta_1$ had little effect on the energy growth relative to Tu, and this is also observed

in the experimental results here. Furthermore, a smaller integral length scale resulted in a higher initial level of disturbance energy in the boundary layer and has also been observed by Hosseinverdi (2014). However, in their work, the saturation of the energy growth was found to be independent of Λ_u. Based on the experimental observations here and past numerical simulations, an effect of the integral length scale could be present, and further investigation is warranted. However, it is likely that the effect will be small compared with Tu, in light of the results here and those from Hosseinverdi & Fasel (2019).

3.2.3. *Co-existence of a modal and a non-modal instabilities*

The assertions made in the previous sections on the co-existence of modal and non-modal growths of disturbances in the LSB will be examined here through a linear stability analysis. Linear stability theory models the amplification of small-amplitude disturbances (Schmid & Henningson 2000) and has been employed to study the convective streamwise amplification of disturbances in the LSB. The Orr–Sommerfeld equation is given by (3.3) and can reliably predict the primary amplification of instability waves for parallel flows and in the fore position of an LSB (Kurelek *et al.* 2018)

$$\left(U-\frac{\Omega}{\alpha}\right)\left(\frac{\mathrm{d}^2\tilde{v}}{\mathrm{d}y^2}-\alpha^2\tilde{v}\right)-\frac{\mathrm{d}^2U}{\mathrm{d}y^2}\tilde{v}=-\frac{iU_e\delta_1}{\alpha Re_{\delta_1}}\left(\frac{\mathrm{d}^4\tilde{v}}{\mathrm{d}y^4}-2\alpha^2\frac{\mathrm{d}^2\tilde{v}}{\mathrm{d}y^2}+\alpha^4\tilde{v}\right), \tag{3.3}$$

where Re_{δ_1} is the Reynolds number based on displacement thickness, $\tilde{v}$ is the wall-normal perturbation, Ω is the angular frequency and the complex wavenumber is defined as $\alpha = \alpha_r + i\alpha_i$, where i is the imaginary unit. When $\alpha_i > 0$, the disturbance is attenuated and amplified when $\alpha_i < 0$.

Calculations were conducted using ONERA's in-house stability code, where a spatial formulation of the problem is employed (Schmid & Henningson 2000), such that Ω is defined and the eigenvalue problem is solved for α, therefore modelling the convective amplification of single frequency disturbances. Equation (3.3) is solved numerically using Chebyshev polynomial base functions and the companion matrix technique to treat eigenvalue nonlinearity (Bridges & Morris 1984).

The mean streamwise velocity profiles at discrete streamwise locations are used as input for the LST calculations, making the analysis local, with the same methodology employed by Yarusevych & Kotsonis (2017) and Kurelek *et al.* (2018). Stability calculations are highly sensitive to noise due to the spatial resolution in experiments. Therefore, the LST analysis is conducted using hyperbolic tangent fits to experimental data, which have shown to provide reasonable stability predictions, being relatively insensitive to scatter in experimental data. The following modified hyperbolic tangent fit was used:

$$\frac{U}{U_e}=\frac{\tanh[a_1(y-a_2)]+\tanh[a_1a_2]}{1+\tanh[a_1a_2]}+a_3\frac{y}{a_2}\exp\left[-1.5\frac{y}{a_2}^2+0.5\right], \tag{3.4}$$

which was proposed by Dovgal, Kozlov & Michalke (1994) and has been shown to suitably model separated boundary-layer profiles in several analytical applications (Boutilier 2011; Boutilier & Yarusevych 2013) along with accurate linear stability predictions on HWA velocity profiles of separated shear layers (Boutilier & Yarusevych 2012). The profile edge velocity, U_e, is estimated from the HWA measurements, while the coefficients $a_1 - a_4$ are estimated through a least-squares curve fitting operation to the measured data. Exemplary velocity profiles and their corresponding fits for the configuration with $Tu = 1.21\,\%$ are presented in figure 15. Furthermore, due to the difficulty in conducting stability calculations on experimental velocity profiles at low Tu and Reynolds numbers,

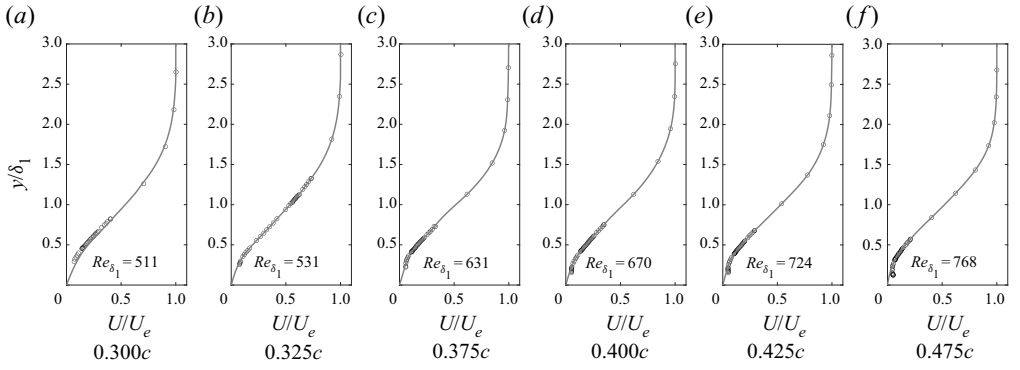

Figure 15. Measured mean velocity profiles (markers) in a forced condition ($Tu = 1.21\,\%$) and corresponding hyperbolic tangent fits (solid lines) used in LST computations.

LST calculations for the baseline case are validated by conducting the analysis on both experimental (hyperbolic fit) and numerical (obtained from the boundary-layer solver, 3C3D) velocity profiles which were within acceptable agreement.

A measure of the amplitude growth is quantified from LST through the computation of amplification factors and will be referred to as the N-factor hereinafter. The N-factor as a function of streamwise position (x) and frequency (F) from LST calculations and is quantified by integrating α_i for the most amplified frequency in the positive x-direction

$$N(x, F) = \int_{x_{cr}}^{x} -\alpha_i \, \mathrm{d}x, \tag{3.5}$$

where x_{cr} is the critical abscissa and corresponds to the location at which a perturbation at a non-dimensional frequency of Ω is first amplified. The location of x_{cr} is upstream of the hot-wire measurement region and, therefore, cannot be determined directly. However, as demonstrated by Jones, Sandberg & Sandham (2010), Kurelek *et al.* (2018), Yarusevych & Kotsonis (2017) and Kurelek (2021), in the fore portion of the LSB the streamwise evolution of α_i can be approximated by a second-order polynomial. For example, Kurelek (2021) (HWA, Ch. 6) and Kurelek *et al.* (2018) (PIV) demonstrated that the $(-\alpha_i)$ obtained from LST calculations for four velocity profiles before and after the separation position could be used in the interpolation. Considering this, x_{cr} can be determined by extrapolating the fit to $\alpha_i = 0$. Experimentally, the N-factor is calculated as $N(x) = \ln(A(x)/A_{cr})$, where $A(x)$ denotes the maximum disturbance amplitude in the boundary layer for a given frequency band (band-pass filtered u_{rms}) and A_{cr} denotes the initial disturbance amplitude that becomes unstable. A direct comparison of N-factor obtained from LST and experiment is not possible since, experimentally, the initial disturbance amplitude is not known and likely to be too small to be measured, only being detected well downstream of x_{cr}. Nevertheless, following Schmid & Henningson (2000), N-factors are matched at a reference location where the disturbance amplitude reaches $0.005U_\infty$, consequently allowing for an estimate of A_{cr} for a given frequency band.

In the baseline configuration, the overlaid plot between PSD and the N-factor shows that LST is capable of predicting the most amplified frequencies from experiment, with acceptable accuracy (10 % difference). For example, Kurelek *et al.* (2018) and Yarusevych & Kotsonis (2017) found a difference of 17 %, while stating this to be an acceptable range. A comparison with experimental N-factors further supports the validity of the LST predictions (cf. figures 16*a* and 17*a*), which reveals that the linear growth of disturbances

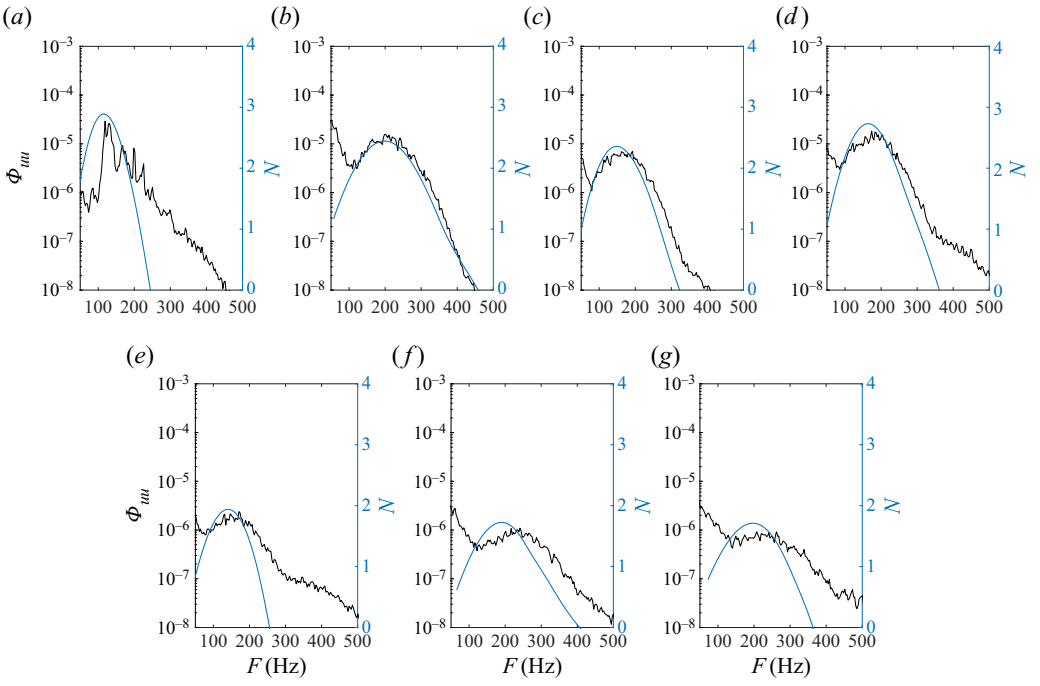

Figure 16. Comparison between the N-factors predicted by LST and the experimental spectra for (a) natural case ($x = 0.400c$); (b) $Tu = 0.64\,\%\,\Lambda_u = 4.6$ mm ($x = 0.425c$); (c) $Tu = 1.21\,\%\,\Lambda_u = 8.7$ mm ($x = 0.425c$); (d) $Tu = 1.23\,\%$, $\Lambda_u = 10.3$ mm ($x = 0.425c$); (f) $Tu = 1.63\,\%$, $\Lambda_u = 12.3$ mm ($x = 0.425c$); (g) $Tu = 2.97\,\%$, $\Lambda_u = 15.4$ mm ($x = 0.400c$). There are two different y-axes for the N-factor and the power from the PSD, therefore direct comparisons between the two are not to be made.

is captured in the range $0.475 < x/c < 0.525$, comparable to the same analysis by Kurelek *et al.* (2018) who found LST to accurately capture the growth of disturbances in the range $0.42 < x/c < 0.46$ in their experiment. Furthermore, as the downstream saturation of the experimental N-factors begins to deteriorate, the agreement between LST due to nonlinear effects becomes significant. The eigenfunction of the most amplified frequency predicted by LST is presented in figure 18(a), and shows acceptable agreement with the experiment for the filtered fluctuating streamwise velocity profile in the wall-normal direction for the most amplified frequency band. The eigenfunction exhibits two distinct peaks at approximately $y/\delta_1 = 1$, corresponding roughly to the inflection point and $y/\delta_1 = 0.3$, which is indicative of a viscous modal instability (Veerasamy *et al.* 2021). Rist & Maucher (2002) showed that Tollmien–Schlichting waves were more likely to emerge in LSBs with small wall-normal distances, and a KH instability in LSBs with higher wall-normal distances. Therefore, based on the agreement seen in the unstable frequencies, eigenfunctions and amplification rates (figures 16a, 18 and 17a), it is established that the employed LST analysis is justified for determining stability characteristics in the fore portion of the LSB.

For the configurations where the LSB is subjected to elevated levels of FST, LST can predict the most amplified frequencies, spatial amplification and eigenfunctions, suggesting that a modal instability is still present at elevated levels of FST when the bubble is present. Counter-intuitively, FST forcing results in better agreement between LST and experiment and has been found in past experiments with increased forcing by Yarusevych

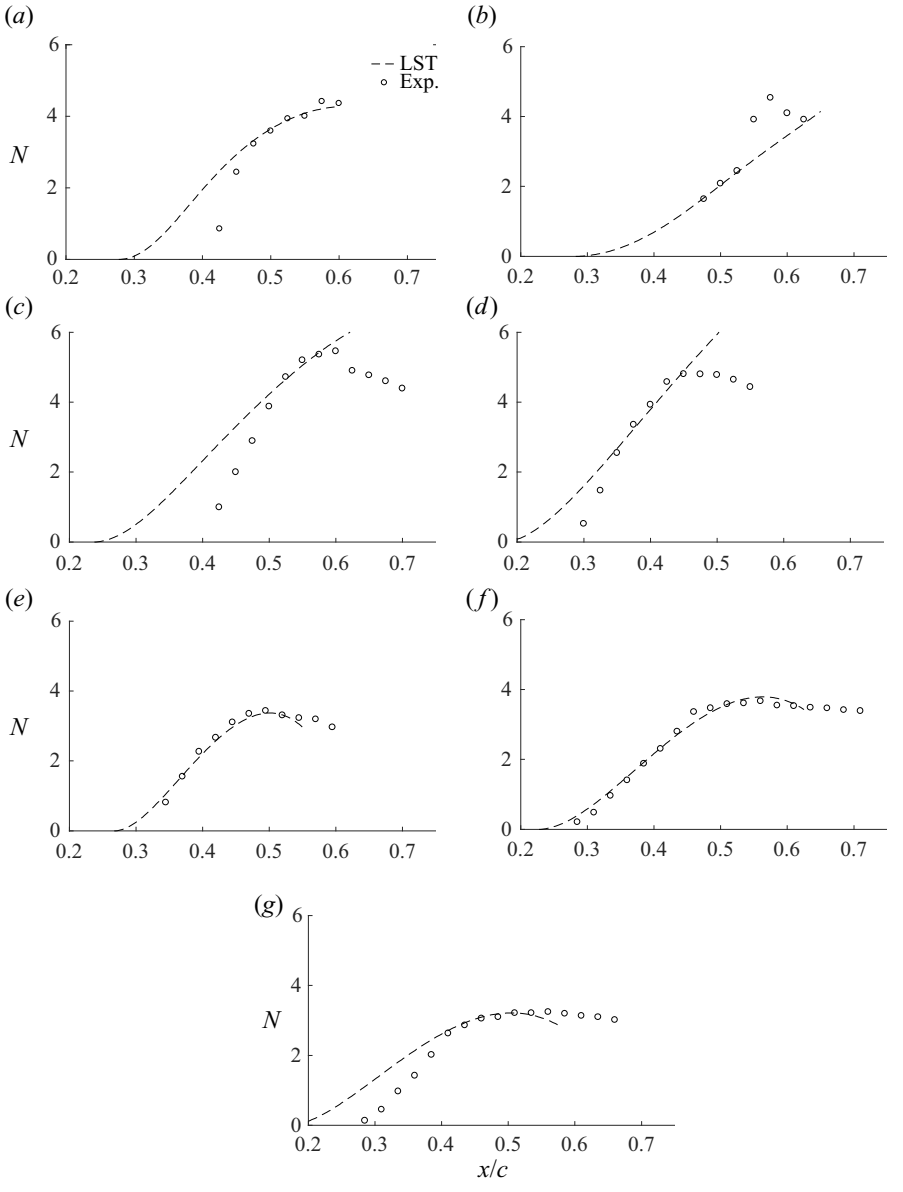

Figure 17. Comparison of experimental (markers) and LST (dashed line) predicted N-factors for frequencies within the excitation bands from figure 10 for configurations where a LSB is present: (*a*) natural case; (*b*) $Tu = 0.64\,\%\, \Lambda_u = 4.6$ mm; (*c*) $Tu = 1.21\,\%$, $\Lambda_u = 8.7$ mm; (*d*) $Tu = 1.23\,\%$, $\Lambda_u = 10.3$ mm; (*e*) $Tu = 1.31\,\%$, $\Lambda_u = 8.3$ mm; (*f*) $Tu = 1.63\,\%$, $\Lambda_u = 12.3$ mm; (*g*) $Tu = 2.97\,\%$, $\Lambda_u = 15.4$ mm; initial disturbance amplitudes are estimated through matching LST and experimental N-factors.

& Kotsonis (2017), Kurelek *et al.* (2018) and Kurelek (2021) (Ch. 6), who found that LST was capable of predicting the convective growth of disturbances in LSBs subjected to plasma, tonal and broadband acoustic forcing. However, as Kurelek *et al.* (2018) noted, the critical caveat to be considered is that the degree to which LST and experiment agree is entirely dictated by the relevance of nonlinear effects for the particular disturbance mode being considered. Fully developed FST could act as a type of 'broadband' forcing, such

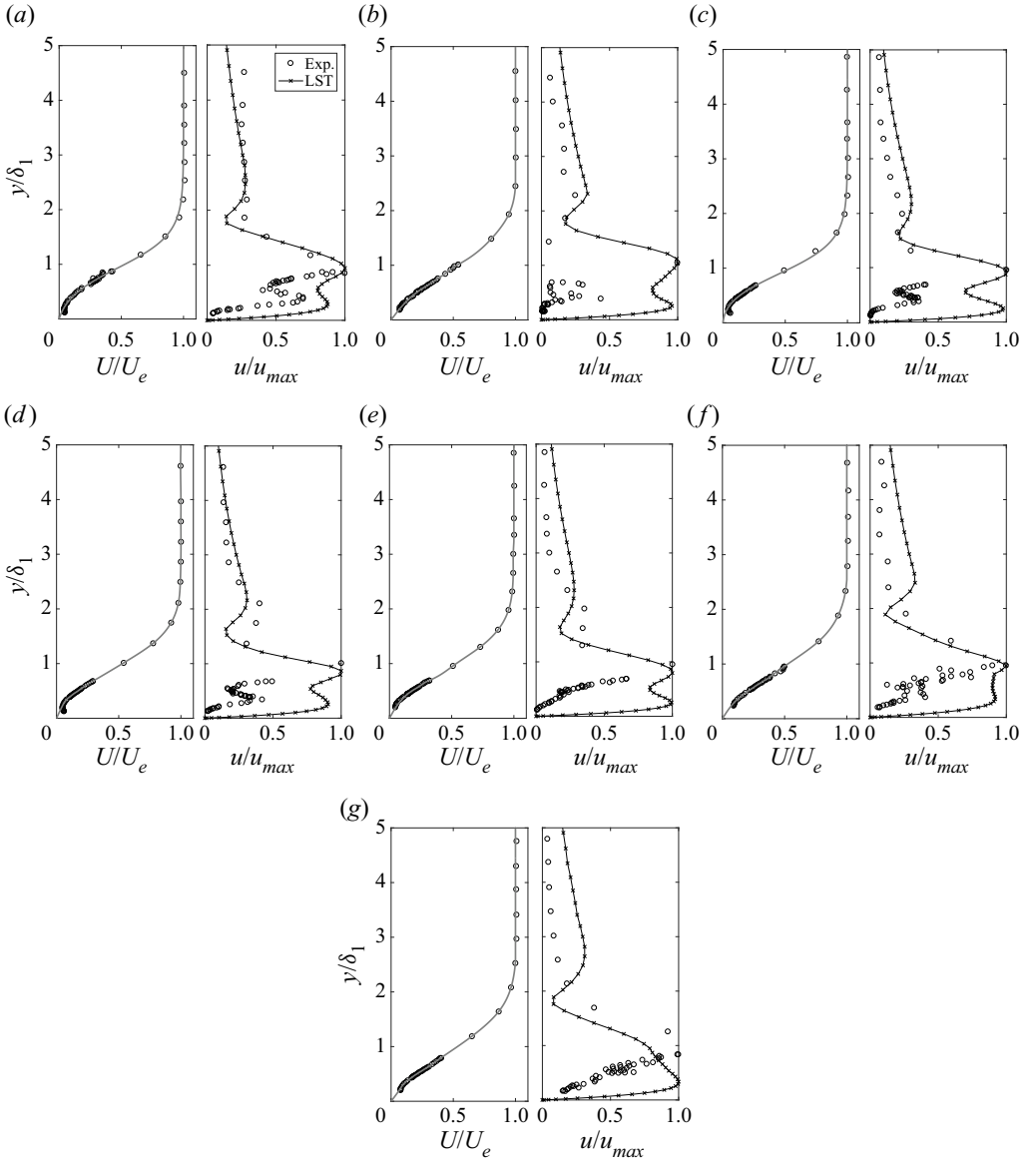

Figure 18. Experimental filtered disturbance profiles in the wall-normal direction compared with the eigenfunction for the most amplified frequency from LST. Experimental streamwise disturbance profiles are computed by applying a bandpass filter corresponding to the lost amplified frequency band from the PSD. (*a*) Natural case; [110–150 Hz] at $x = 0.425c$, (*b*) $Tu = 0.64\,\%$, $\Lambda_u = 4.6$ mm [160–200 Hz] at $x = 0.400c$, (*c*) $Tu = 1.21\,\%$, $\Lambda_u = 8.7$ mm [180–220 Hz] at $x = 0.425c$, (*d*) $Tu = 1.23\,\%$, $\Lambda_u = 10.3$ mm [180–220 Hz] at $x = 0.400c$, (*e*) $Tu = 1.31\,\%$, $\Lambda_u = 8.3$ mm [180–220 Hz] at $x = 0.400c$, (*f*) $Tu = 1.63\,\%$, $\Lambda_u = 12.3$ mm [180–220 Hz] at $x = 0.450c$ and (*g*) $Tu = 2.97\,\%$, $\Lambda_u = 15.4$ mm [255–295 Hz] at $x = 0.425c$.

that all unstable disturbance amplitudes are small, resulting in nonlinear effects and an improved agreement between LST and experiment. Therefore, current results support the assertions made by Kurelek *et al.* (2018), who found excellent agreement between LST and experiment for an LSB subjected to broadband acoustic forcing. The higher signal-to-noise ratio can also explain the improvement in the presence of forcing with FST.

Another explanation for the divergence between LST and experiment for configurations subjected to low levels of Tu could result from the bubble's wall-normal extent being larger compared with higher levels of Tu. The more considerable distance of the shear layer from the wall would foster other instabilities, such as a global oscillator (Rist & Maucher 2002) or even the global oscillator being preceded by the 3-D global instability as in Rodríguez *et al.* (2021). Another possibility could be that a shear on structures in the direction opposed to the mean flow may lead to a non-modal instability through an Orr mechanism (Cherubini, Robinet & De Palma 2010). Therefore, the augmented agreement between LST N-factor envelopes and experiments in configurations subjected to moderate levels of Tu ($1.3\,\% < Tu < 2.97\,\%$) can be explained by these FST levels being effective in exciting Tollmien–Schlichting waves in the pre-separated shear layer. At these moderate Tu levels, the nonlinear distortion of the mean flow due to the streaks does not impact their amplification, resulting in the Orr–Sommerfeld equation predicting the N-factor envelopes from experiment. At a high enough Tu threshold, the mean-flow modification due to the presence of streaks is too significant, resulting in the growth of wave-like disturbances being inhibited and the divergence from LST and experiment.

Consequently, using the analysis employed by Yarusevych & Kotsonis (2017), Kurelek *et al.* (2018) and Kurelek (2021), the current results show that LST is capable of modelling the convective growth of disturbances in a bubble subjected to moderate FST levels. The critical difference is that forcing with elevated levels of FST ($Tu > 1\,\%$) can cause the generation of streaks, considered to be a convective non-modal amplification of disturbances (Matsubara & Alfredsson 2001; Fransson *et al.* 2005; Fransson & Shahinfar 2020). The disturbance profiles just before and after separation presented in figure 19 (non-modal) strongly suggest the existence of the non-modal growth or streaks (Klebanoff modes) as the profiles exhibit self-similar behaviour with the optimal disturbance profiles from the theoretical work of Andersson *et al.* (1999) and Luchini (2000), with the maximum value of u_{rms} occurring near $y/\delta_1 = 1.3$ for all configurations with $Tu > 1\,\%$. The current results demonstrate the self-similarity of the disturbance profiles over most of the boundary layer (cf. figure 19f–j). Outside the boundary layer, results do not tend to zero since FST is present, in contrast to theory, which has no free-stream disturbances outside the boundary layer. Furthermore, inside the LSB, the disturbance profiles also appear to agree well with theory. The slight downwards shift of the profile at the most advanced chordwise positions is due to the flow finishing the transition process. These observations made in figures 18 and 19(f–j, non-modal) implies the co-existence of both modal and non-modal instability mechanisms, confirming the observations in DNS (Hosseinverdi & Fasel 2019) and experimental investigations (Istvan & Yarusevych 2018; Verdoya *et al.* 2021) on LSBs subjected to FST, along with the experimental results of Veerasamy *et al.* (2021) for an attached boundary layer developing over a flat plate. In contrast, in configurations where $Tu < 1\,\%$ (refer to figure 19(a–e), modal), wall-normal disturbance profiles do not agree with theoretical predictions and do not exhibit the same behaviour as for configurations with $Tu > 1\,\%$, with the maxima of the peaks being in the range $y/\delta_1 = 0.3$–0.5, implying that there is no formation of streaks and that only a modal transition mechanism is present. The observation of damping behaviour on the disturbance growth presented in the previous section (figure 13) being due to the non-modal amplification of streaks is supported by the results in figure 19. The damping of disturbance growth in the bubble is also reflected in the LST predictions, as values of amplification are slightly lower for configurations subjected to elevated levels of FST, in line with what has been observed for laminar separation bubbles subjected to other methods of forcing (Marxen & Henningson 2011; Marxen *et al.* 2015; Yarusevych &

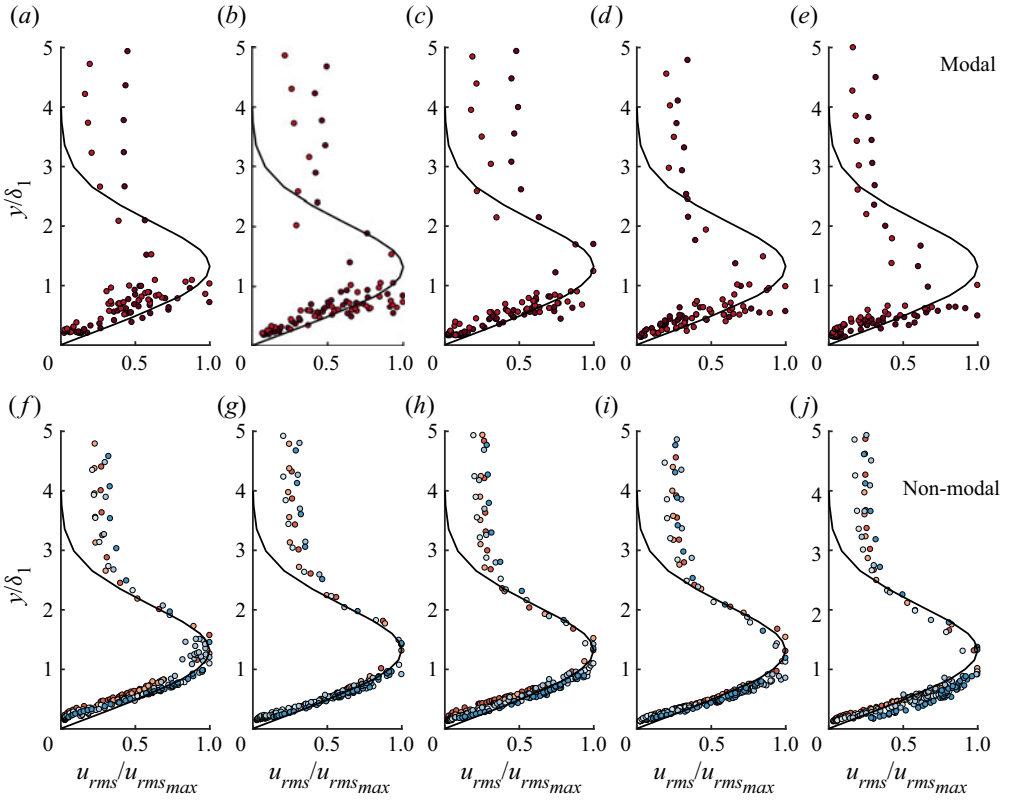

Figure 19. Streamwise velocity disturbance profiles for configurations where LSB is subjected to turbulence of $Tu < 1\,\%$ (*a–e*) and $Tu > 1\,\%$ (*g–k*) for chordwise positions of (*a*,*f*) 0.325*c* (*b*,*g*) 0.350*c* (*c*,*h*) 0.375*c* (*d*,*i*) 0.400*c* and (*e*, *j*) 0.425*c*. Configurations with $Tu < 1\,\%$: NG and C0 and $Tu > 1\,\%$: C1–C5. Refer to table 2 for symbols.

Kotsonis 2017; Kurelek *et al.* 2018). The damping of the convective disturbance growth is due to the streaks modifying the mean flow. Therefore, the wall-normal distance and the length of the LSB is reduced. This results in lower values of δ_1 resulting in lower levels of modal amplification due to the increased viscosity effects.

One may argue that a more rigorous characterisation could be made with fine spanwise hot-wire measurements, however, this was not possible due to the experimental set-up. Nevertheless, the claim of the presence of streaks is valid based on the disturbance profiles (cf. figure 19), decreased energy growth rates (cf. figure 13) and observations from previous work.

Finally, when the bubble is subjected to a sufficient level of FST forcing ($Tu > 3\,\%$, in the present configuration), the formation of an LSB is not observed in the experimental data, suggesting that there is a critical initial forcing amplitude which will generate streaks containing enough energy to suppress boundary-layer separation by promoting earlier transition. Figure 20 confirms the existence of non-modal instabilities growing in the streamwise direction for the values of *Tu* where no separation was observed. Streamwise velocity disturbance profiles are in very good agreement with Andersson *et al.* (1999) and Luchini (2000), exhibiting a clear peak at $y/\delta_1 \approx 1.3$, with profiles further downstream manifesting a lower wall-normal position of the maxima due to the flow undergoing transition and tending to a turbulent state where the peak in the fluctuating

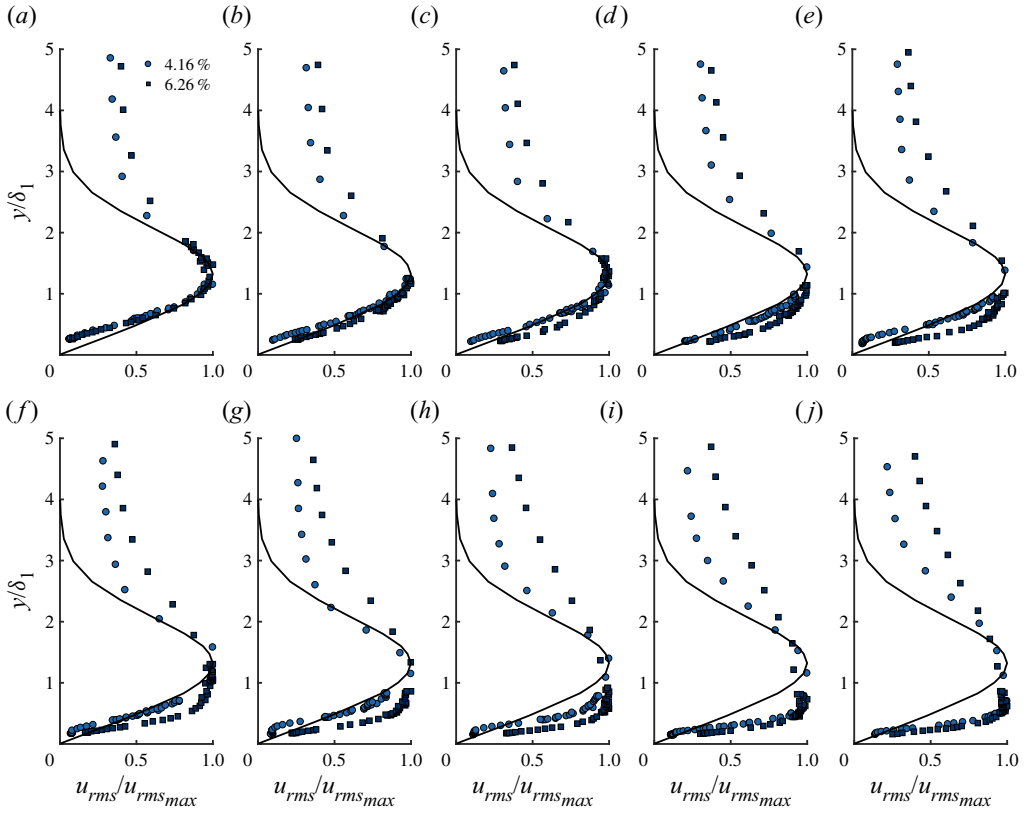

Figure 20. Chordwise evolution of the disturbance profiles scaled with $u_{rms,max}$ for chordwise positions of (*a*) 0.250*c*, (*b*) 0.300*c*, (*c*) 0.325*c*, (*d*) 0.350*c*, (*e*) 0.375*c*, (*f*) 0.400*c*, (*g*) 0.425*c*, (*h*) 0.450*c*, (*i*) 0.475*c*, (*j*) 0.500*c*. Black line denoted theoretical optimal perturbation profile by Luchini (2000). Configurations C6 and C7: refer to table 2 for symbols.

velocity component is closer to the wall. Furthermore, the u_{rms} profiles exhibit no peaks below $y/\delta_1 \approx 1.3$, in stark contrast to what is observed in configurations containing a LSB. At the highest levels of FST, the bubble could be suppressed due to the boundary layer transitioning before the strong adverse pressure-gradient region, which promotes separation. However, the results could also suggest the suppression of laminar separation due to streaks (at least for the current experimental configuration), which is supported by the recent numerical investigation by Xu & Wu (2021). They found that free-stream vortical disturbances of moderate level prevent the separation in a boundary-layer flow over a plate or concave wall, suggesting that the strong mean-flow distortion associated with the nonlinear streaks or Görtler vortices prevents separation. The simulations by Xu & Wu (2021) found that streaks with maximum amplitudes of approximately 12 % suppressed separation, whereas, at lower amplitudes, separation would still occur. A similar phenomenon could exist in our results, where critically energetic streaks generated by sufficiently elevated FST can suppress separation. In these cases, as in Xu & Wu (2021), we also observe streak amplitudes in the range of 10 %–15 % of the free-stream velocity, although, at lower amplitudes, an LSB is still present.

4. Concluding remarks

The present investigation examines the effects of varying the free-stream turbulence intensity and integral length scale on the flow development and transition in a LSB. The LSB develops over the suction side of a NACA0015 aerofoil at a chord-based Reynolds number of 125 000 and angle of incidence of 2.3° in a low FST open circuit wind tunnel. Free-stream turbulence was generated in a controlled manner using regular and fractal grids resulting in a wide range of levels of turbulence intensity and integral length scales. The streamwise evolution of FST and the flow field were characterised using HWA. Eight free-stream flow configurations were tested, three with a fixed turbulence intensity level but a variable integral length scale.

The results exhibit that elevated levels of FST reduce the size of the mean bubble flow topology, advancing the transition position and decreasing the size of the bubble, with its eventual elimination at the highest levels. In the LSB, the convective development of an unstable frequency band is observed and is broadened with the addition of FST, a consequence of more significant energy content within a broader range of frequencies from the FST. The presence of FST also shifts the most amplified frequency band to a higher spectral range due to smaller wall-normal and streamwise lengths of the bubble when excited. In the baseline case, when the most amplified frequencies are non-dimensionalised through the use of a Strouhal number based on the boundary-layer momentum thickness at separation, $St_{\delta_{2,sep}}$, an agreement is found with Pauley *et al.* (1990). However, increasing Tu causes $St_{\delta_{2,sep}}$ to increase when compared with the baseline case, approaching values closer to what was observed by Rodríguez *et al.* (2021).

The presence of streaks is observed for configurations with $Tu > 1\,\%$, with unfiltered profiles agreeing remarkably well with the theoretical optimal perturbation profile at multiple chordwise positions before and inside the LSB. The mechanism of disturbance energy growth gradually changes from an exponential one, at lower levels of Tu, to an algebraic one for the more extreme Tu levels, growing until the energy saturates. In the configuration where a bubble is present, band-pass filtered (corresponding to the most amplified frequency range) values of disturbance energy reveal the gradual reduction in the slope of the chordwise energy growth with increasing Tu, suggesting that the non-modal instabilities become more dominant, which can be thought of as competing with the modal instabilities. Once the turbulence forcing reaches a critical level, $Tu \approx 4\,\%$ in the present study, the streaks in the boundary layer are too energetic to allow the flow to separate, ensuing in the elimination of the modal instability via the non-modal instability and suppressing the formation of the bubble. The damping of the streamwise growth of disturbances is due to the presence of streaks (Klebanoff modes) caused by the elevated levels of FST, which change the mean-flow topology of the bubble through the introduction of non-modal disturbances into the boundary layer. Finally, for a relatively fixed level of Tu, the variation of Λ_u has modest effects; however, a slight advancement of transition with the decrease in Λ_u is observed.

Local linear stability analysis is shown to accurately model incipient distance growth for the unexcited turbulence case, in agreement with previous work (Yarusevych & Kotsonis 2017; Kurelek *et al.* 2018; Kurelek 2021). Moreover, good agreement between LST eigenfunctions and filtered experimental u_{rms} profiles and the prediction of the most amplified frequencies is found. In the presence of elevated turbulence, LST predicts the growth of disturbances and unstable frequencies with acceptable accuracy. Counter-intuitively, an augmented agreement between experiment and LST for N-factor envelopes was present in configurations subjected to moderate levels of FST and was

thought to be due to the turbulence being effective in exciting the viscous modal instabilities in the pre-separated shear layer. Additionally, filtered u_{rms} profiles were representative of those predicted by LST and resembled those which are expected in the presence of modal visco-inflectional instabilities. Therefore, the current work provides rigorous experimental evidence on the co-existence of modal and non-modal instabilities in a laminar separation bubble.

Funding. Supported by internal funding of ONERA and ISAE–SUPAERO.

Declaration of interests. The authors report no conflict of interest.

Author ORCIDs.
Tomek Jaroslawski https://orcid.org/0000-0003-0235-9888;
Olivier Vermeersch https://orcid.org/0000-0003-3385-7951;
Erwin R. Gowree https://orcid.org/0000-0002-4475-5996.

References

ANDERSSON, P., BERGGREN, M. & HENNINGSON, D.S. 1999 Optimal disturbances and bypass transition in boundary layers. *Phys. Fluids* **11** (1), 134–150.

ARNAL, D. & JULIEN, J.C. 1978 Contribution expérimentale à l'etude de la receptivité d'une couche limite laminaire, à la turbulence de l'écoulement generale. *Tech. Rep.* 1/5018 AYD.

BALZER, W. & FASEL, H. 2016 Numerical investigation of the role of free-stream turbulence in boundary-layer separation. *J. Fluid Mech.* **801**, 289–321.

BENEDICT, L.H. & GOULD, R.D. 1996 Towards better uncertainty estimates for turbulence statistics. *Exp. Fluids* **22** (2), 129–136.

BOUTILIER, M.S.H. & YARUSEVYCH, S. 2012 Separated shear layer transition over an airfoil at a low Reynolds number. *Phys. Fluids* **24** (8), 084105.

BOUTILIER, M.S.H. & YARUSEVYCH, S. 2013 Sensitivity of linear stability analysis of measured separated shear layers. *Eur. J. Mech. (*B*/Fluids)* **37**, 129–142.

BOUTILIER, M.S.H. 2011 Experimental investigation of transition over a NACA 0018 airfoil at a low Reynolds number. Master's thesis, University of Waterloo.

BRANDT, L., SCHLATTER, P. & HENNINGSON, D.S. 2004 Transition in boundary layers subject to free-stream turbulence. *J. Fluid Mech.* **517**, 167.

BREUER, M. 2018 Effect of inflow turbulence on an airfoil flow with laminar separation bubble: an LES study. *Flow Turbul. Combust.* **101** (2), 433–456.

BRIDGES, T.J. & MORRIS, P.J. 1984 Differential eigenvalue problems in which the parameter appears nonlinearly. *J. Comput. Phys.* **55** (3), 437–460.

BRUUN, H.H. 1996 *Hot-wire Anemometry: Principles and Signal Analysis*. Oxford University Press.

BURATTINI, P. & ANTONIA, R.A. 2005 The effect of different X-wire calibration schemes on some turbulence statistics. *Exp. Fluids* **38** (1), 80–89.

BURGMANN, S. & SCHRÖDER, W. 2008 Investigation of the vortex induced unsteadiness of a separation bubble via time-resolved and scanning PIV measurements. *Exp. Fluids* **45** (4), 675–691.

CARMICHAEL, B.H. 1981 Low Reynolds number airfoil survey, volume 1. *NASA Contractor Rep.* 165803.

CHERUBINI, S., ROBINET, J.-CH. & DE PALMA, P. 2010 The effects of non-normality and nonlinearity of the Navier–Stokes operator on the dynamics of a large laminar separation bubble. *Phys. Fluids* **22** (1), 014102.

DELLACASAGRANDE, M., BARSI, D., LENGANI, D., SIMONI, D. & VERDOYA, J. 2020 Response of a flat plate laminar separation bubble to Reynolds number, free-stream turbulence and adverse pressure gradient variation. *Exp. Fluids* **61** (6).

DIWAN, S.S. & RAMESH, O.N. 2009 On the origin of the inflectional instability of a laminar separation bubble. *J. Fluid Mech.* **629**, 263–298.

DOVGAL, A.V., KOZLOV, V.V. & MICHALKE, A. 1994 Laminar boundary layer separation: instability and associated phenomena. *Prog. Aerosp. Sci.* **30** (1), 61–94.

DRELA, M. 1989 XFOIL: an analysis and design system for low Reynolds number airfoils. In *Low Reynolds Number Aerodynamics* (ed. T.J. Mueller), Lecture Notes in Engineering, vol. 54, pp. 1–12. Springer.

FRANSSON, J.H.M., MATSUBARA, M. & ALFREDSSON, P.H. 2005 Transition induced by free-stream turbulence. *J. Fluid Mech.* **527**, 1–25.

FRANSSON, J.H.M. & SHAHINFAR, S. 2020 On the effect of free-stream turbulence on boundary-layer transition. *J. Fluid Mech.* **899**, A23.
GASTER, M. 1967 The structure and behaviour of laminar separation bubbles. *Tech. Rep.* 3595. Aeronautical Research Council.
HÄGGMARK, C.P., BAKCHINOV, A.A. & ALFREDSSON, P.H. 2000 Experiments on a two–dimensional laminar separation bubble. *Phil. Trans. R. Soc. Lond.* A **358** (1777), 3193–3205.
HÄGGMARK, C.P., HILDINGS, C. & HENNINGSON, D.S. 2001 A numerical and experimental study of a transitional separation bubble. *Aerosp. Sci. Technol.* **5** (5), 317–328.
HISLOP, G.S. 1940 The transition of a laminar boundary layer in a wind tunnel. PhD thesis, University of Cambridge.
HOSSEINVERDI, S. 2014 Influence of free-stream turbulence on laminar-turbulent transition in long laminar separation bubbles: direct numerical simulations. Master's thesis, University of Arizona.
HOSSEINVERDI, S. & FASEL, H. 2019 Numerical investigation of laminar–turbulent transition in laminar separation bubbles: the effect of free-stream turbulence. *J. Fluid Mech.* **858**, 714–759.
HOUDEVILLE, R. 1992 Three-dimensional boundary layer calculation by a characteristic method. In *Fifth Symposium on Numerical and Physical Aspects of Aerodynamic Flows, Long Beach, January 1992*. California State University.
HURST, D. & VASSILICOS, J.C. 2007 Scalings and decay of fractal-generated turbulence. *Phys. Fluids* **19** (3), 035103.
ISTVAN, M.S. & YARUSEVYCH, S. 2018 Effects of free-stream turbulence intensity on transition in a laminar separation bubble formed over an airfoil. *Exp. Fluids* **59** (3), 52.
JAROSLAWSKI, T., FORTE, M., MOSCHETTA, J.-M., DELATTRE, G. & GOWREE, E.R. 2022 Characterisation of boundary layer transition over a low Reynolds number rotor. *Exp. Therm. Fluid Sci.* **130**, 110485.
JONÁŠ, P., MAZUR, O. & URUBA, V. 2000 On the receptivity of the by-pass transition to the length scale of the outer stream turbulence. *Eur. J. Mech. (*B*/Fluids)* **19** (5), 707–722.
JONES, L.E., SANDBERG, R.D. & SANDHAM, N.D. 2010 Stability and receptivity characteristics of a laminar separation bubble on an aerofoil. *J. Fluid Mech.* **648**, 257–296.
KENDALL, J. 1998 Experiments on boundary-layer receptivity to freestream turbulence. *AIAA Paper* 98-0530.
KLEBANOFF, P.S. & TIDSTROM, K.D. 1972 Mechanism by which a two-dimensional roughness element induces boundary-layer transition. *Phys. Fluids* **15** (7), 1173–1188.
KURELEK, J. 2021 The vortex dynamics of laminar separation bubbles. PhD thesis, University of Waterloo.
KURELEK, J.W., KOTSONIS, M. & YARUSEVYCH, S. 2018 Transition in a separation bubble under tonal and broadband acoustic excitation. *J. Fluid Mech.* **853**, 1–36.
KURELEK, J.W., LAMBERT, A.R. & YARUSEVYCH, S. 2016 Coherent structures in the transition process of a laminar separation bubble. *AIAA J.* **54** (8), 2295–2309.
KURIAN, T. & FRANSSON, J.H.M. 2009 Grid-generated turbulence revisited. *Fluid Dyn. Res.* **41** (2), 021403.
LI, H.J. & YANG, Z. 2019 Separated boundary layer transition under pressure gradient in the presence of free-stream turbulence. *Phys. Fluids* **31** (10), 104106.
LUCHINI, P. 2000 Reynolds-number-independent instability of the boundary layer over a flat surface: optimal perturbations. *J. Fluid Mech.* **404**, 289–309.
LUEPTOW, R.M., BREUER, K.S. & HARITONIDIS, J.H. 2004 Computer-aided calibration of X-probes using a look-up table. *Exp. Fluids* **6** (2), 115–118.
MAKITA, H. & SASSA, K. 1991 Active turbulence generation in a laboratory wind tunnel. In *Advances in Turbulence 3* (ed. A.V. Johansson & P.H. Alfredsson), pp. 497–505. Springer.
MAMIDALA, S.B., WEINGÄRTNER, A. & FRANSSON, J.H.M. 2022 Leading-edge pressure gradient effect on boundary layer receptivity to free-stream turbulence. *J. Fluid Mech.* **935**, A30.
MARXEN, O. & HENNINGSON, D.S. 2011 The effect of small-amplitude convective disturbances on the size and bursting of a laminar separation bubble. *J. Fluid Mech.* **671**, 1–33.
MARXEN, O., KOTAPATI, R.B., MITTAL, R. & ZAKI, T. 2015 Stability analysis of separated flows subject to control by zero-net-mass-flux jet. *Phys. Fluids* **27** (2), 024107.
MARXEN, O., LANG, M. & RIST, U. 2013 Vortex formation and vortex breakup in a laminar separation bubble. *J. Fluid Mech.* **728**, 58–90.
MARXEN, O., LANG, M., RIST, U. & WAGNER, S. 2003 A combined experimental/numerical study of unsteady phenomena in a laminar separation bubble. *Flow Turbul. Combust.* **71** (1–4), 133–146.
MATSUBARA, M. & ALFREDSSON, P.H. 2001 Disturbance growth in boundary layers subjected to free-stream turbulence. *J. Fluid Mech.* **430**, 149.
MICHELIS, T., YARUSEVYCH, S. & KOTSONIS, M. 2017 Response of a laminar separation bubble to impulsive forcing. *J. Fluid Mech.* **820**, 633–666.

MORKOVIN, M.V. 1985 Bypass transition to turbulence and research desiderata. *Trans. Turbines* **2386**, 161–204.

NOLAN, K.P., WALSH, E.J. & MCELIGOT, D.M. 2010 Quadrant analysis of a transitional boundary layer subject to free-stream turbulence. *J. Fluid Mech.* **658**, 310.

OLSON, D.A., KATZ, A.W., NAGUIB, A.M., KOOCHESFAHANI, M.M., RIZZETTA, D.P. & VISBAL, M.R. 2013 On the challenges in experimental characterization of flow separation over airfoils at low Reynolds number. *Exp. Fluids* **54** (2), 1–11.

OVCHINNIKOV, V., CHOUDHARI, M.M. & PIOMELLI, U. 2008 Numerical simulations of boundary-layer bypass transition due to high-amplitude free-stream turbulence. *J. Fluid Mech.* **613**, 135–169.

PAULEY, L.L. 1994 Structure of local pressure-driven three-dimensional transient boundary-layer separation. *AIAA J.* **32** (5), 997–1005.

PAULEY, L.L., MOIN, P. & REYNOLDS, W.C. 1990 The structure of two-dimensional separation. *J. Fluid Mech.* **220**, 397–411.

RIST, U. & MAUCHER, U. 2002 Investigations of time-growing instabilities in laminar separation bubbles. *Eur. J. Mech. (*B*/Fluids)* **21** (5), 495–509.

RODRÍGUEZ, D. & GENNARO, E.M. 2019 Enhancement of disturbance wave amplification due to the intrinsic three-dimensionalisation of laminar separation bubbles. *Aeronaut. J.* **123** (1268), 1492–1507.

RODRÍGUEZ, D., GENNARO, E.M. & JUNIPER, M.P. 2013 The two classes of primary modal instability in laminar separation bubbles. *J. Fluid Mech.* **734**, R4.

RODRÍGUEZ, D., GENNARO, E.M. & SOUZA, L.F. 2021 Self-excited primary and secondary instability of laminar separation bubbles. *J. Fluid Mech.* **906**, A13.

RODRÍGUEZ, D. & THEOFILIS, V. 2010 Structural changes of laminar separation bubbles induced by global linear instability. *J. Fluid Mech.* **655**, 280–305.

SCHMID, P.J. & HENNINGSON, D.S. 2000 *Stability and Transition in Shear Flows*, vol. 142. Springer Science & Business Media.

SERNA, J. & LÁZARO, B.J. 2014 The final stages of transition and the reattachment region in transitional separation bubbles. *Exp. Fluids* **55** (4), 1–17.

SIMONI, D., LENGANI, D., UBALDI, M., ZUNINO, P. & DELLACASAGRANDE, M. 2017 Inspection of the dynamic properties of laminar separation bubbles: free-stream turbulence intensity effects for different Reynolds numbers. *Exp. Fluids* **58** (6), 66.

STUDER, G., ARNAL, D., HOUDEVILLE, R. & SERAUDIE, A. 2006 Laminar–turbulent transition in oscillating boundary layer: experimental and numerical analysis using continuous wavelet transform. *Exp. Fluids* **41** (5), 685–698.

VEERASAMY, D., ATKIN, C.J. & PONNUSAMI, S.A. 2021 Aerofoil wake-induced transition characteristics on a flat-plate boundary layer. *J. Fluid Mech.* **920**, A29.

VERDOYA, J., DELLACASAGRANDE, M., LENGANI, D., SIMONI, D. & UBALDI, M. 2021 Inspection of structures interaction in laminar separation bubbles with extended proper orthogonal decomposition applied to multi-plane particle image velocimetry data. *Phys. Fluids* **33** (4), 043607.

VOLINO, R.J. 1998 A new model for free-stream turbulence effects on boundary layers. *ASME. J. Turbomach.* **120** (3), 613–620.

WATMUFF, J.H. 1999 Evolution of a wave packet into vortex loops in a laminar separation bubble. *J. Fluid Mech.* **397**, 119–169.

WESTIN, K.J.A., BOIKO, A.V., KLINGMANN, B.G.B., KOZLOV, V.V. & ALFREDSSON, P.H. 1994 Experiments in a boundary layer subjected to free stream turbulence. Part 1. Boundary layer structure and receptivity. *J. Fluid Mech.* **281**, 193–218.

WISSINK, J.G. & RODI, W. 2006 Direct numerical simulations of transitional flow in turbomachinery. *J. Turbomach.* **128** (4), 668–667.

XU, D. & WU, X. 2021 Elevated low-frequency free-stream vortical disturbances eliminate boundary-layer separation. *J. Fluid Mech.* **920**, A14.

XU, H., MUGHAL, S.M., GOWREE, E.R., ATKIN, C.J. & SHERWIN, S.J. 2017 Destabilisation and modification of Tollmien–Schlichting disturbances by a three-dimensional surface indentation. *J. Fluid Mech.* **819**, 592–620.

YARUSEVYCH, S. & KOTSONIS, M. 2017 Steady and transient response of a laminar separation bubble to controlled disturbances. *J. Fluid Mech.* **813**, 955–990.

ZAMAN, K.B.M.Q., MCKINZIE, D.J. & RUMSEY, C.L. 1989 A natural low-frequency oscillation of the flow over an airfoil near stalling conditions. *J. Fluid Mech.* **202**, 403–442.